JGR Solid Earth

Key Points:

- Locally increased fluid pressure can generate four types of fault slip behaviors distinguished by slow slip events (SSEs) and earthquake initiation mode
- SSEs with extremely high peak slip rates have the potential to nucleate huge earthquakes
- There is no threshold in peak slip rate for SSEs to trigger the nucleation of regular earthquakes

Correspondence to:

K. Xia,
kaiwen.xia@utoronto.ca

Author Contributions:

Conceptualization: Peng Dong, Kaiwen Xia
Data curation: Peng Dong
Formal analysis: Peng Dong, Ran Xu, Hongfeng Yang
Funding acquisition: Hongfeng Yang, Kaiwen Xia
Investigation: Peng Dong, Ran Xu, Zhiyin Guo
Methodology: Peng Dong
Supervision: Kaiwen Xia
Visualization: Peng Dong, Ran Xu
Writing – original draft: Peng Dong
Writing – review & editing: Hongfeng Yang, Kaiwen Xia

Fault Slip Behaviors Modulated by Locally Increased Fluid Pressure: Earthquake Nucleation and Slow Slip Events

Peng Dong[1,2] , **Ran Xu[3]**, **Hongfeng Yang[4]** , **Zhiyin Guo[3]**, and **Kaiwen Xia[1,2,3]**

[1]Institute of Geosafety, School of Engineering and Technology, China University of Geosciences, Beijing, China, [2]Department of Civil and Mineral Engineering, University of Toronto, Toronto, ON, Canada, [3]State Key Laboratory of Hydraulic Engineering Simulation and Safety, School of Civil Engineering, Tianjin University, Tianjin, China, [4]Earth System Science Programme, The Chinese University of Hong Kong, Hong Kong, China

Abstract Huge earthquakes are frequently preceded by slow slip events (SSEs) that are speculated as the precursor to regular earthquakes (REs). However, the way in which earthquakes initiate, as well as the interactions between SSEs and REs remain poorly understood, adding more mysteries to the initiation of earthquakes. Here, we perform systematic numerical simulations to explore the relationships between SSEs and REs on faults including locally increased fluid pressure. We identify four types of fault slip behaviors distinguished by SSE and earthquake initiation mode. The observed interactions between SSEs and REs share similar features with those reported for natural earthquakes. Our results show that the occurrence of SSEs may temporarily hasten fault decoupling, leading to the clock advance of mainshocks. Furthermore, the interactions between SSEs and REs are more complicated than previously thought. On the one hand, since SSEs with extremely high peak slip rates tend to directly transform into huge earthquakes, the possibility of huge earthquakes may increase when SSEs happen. On the other hand, there is no threshold in peak slip rate for SSEs to trigger the nucleation of REs. Therefore, it is difficult to distinguish the SSEs that could trigger a huge earthquake from regular ones only with the knowledge of the peak slip rate. We also verify that the spatial extent of SSEs is related to the occurrence of earthquakes to some extent. These findings may have major implications for understanding the interactions between SSEs and REs, and the mechanism of earthquake initiation.

Plain Language Summary Some earthquakes are reported to be preceded by slow slip events (SSEs). These SSEs are regarded as the precursor to earthquakes. However, not all SSEs are followed by earthquakes, making the prediction of earthquakes based on the monitoring of SSEs unreliable. In this paper, we explore the relationships between SSEs and REs, based on numerical simulations. Locally increased fluid pressure is included on the fault to generate SSEs. We identify four types of fault slip behaviors distinguished by SSE and earthquake initiation mode. Some earthquakes are triggered by SSEs and some SSEs can directly transform into earthquakes. Although we find that SSEs with high peak slip rates tend to transform into huge earthquakes, leading to an increased likelihood of large earthquakes, SSEs with very low slip rates can still trigger the nucleation of earthquakes. The result suggests that the prediction of earthquakes cannot solely rely on the peak slip rate of SSEs. The spatial extent of SSEs is correlated with the occurrence of REs. The results suggest that the study of slow slip and its connections between earthquakes may help us better understand the mechanics of natural earthquakes.

1. Introduction

Facilitated by the improvements of geodetic and seismic observation networks, a spectrum of unusual slow earthquakes has been discovered, including very low-frequency earthquakes, short- and long-term slow slip events (SSEs), and episodic tremor and slip (Ide et al., 2007; Obara & Kato, 2016; Peng & Gomberg, 2010; Rogers & Dragert, 2003). The discovery of slow earthquakes manifests the complexity of fault slip behaviors, ranging from aseismic creep to seismic events. The studies of slow earthquakes may provide insights into the fault slip budget and its temporal variation over time, which is of fundamental importance to our understanding of the physics of earthquakes.

Among these slow earthquakes, SSEs are usually defined as temporary episodes of creep acceleration with a duration of days to years (Obara & Kato, 2016). SSEs slip too slowly to radiate seismic waves, but sometimes

are accompanied by episodic tremors or microshocks, facilitating the detection and characterization of SSEs (Ito et al., 2007). Recent advances in observations reveal that SSEs occur in different tectonic settings worldwide, primarily in the subduction zones (Dragert et al., 2001; H. Hirose et al., 1999; Miller et al., 2002; Ozawa et al., 2002; Wallace et al., 2016) and transform plate boundary faults (Khoshmanesh et al., 2015; Linde et al., 1996; Nadeau & McEvilly, 2004; Shelly, 2009). Generally, SSEs are located shallower or deeper than the seismogenic zone, or near the strongly locked segments of the faults. Sometimes, SSEs can migrate toward the locked segments of megathrust (Uchida et al., 2020) or even penetrate the seismic patch (Ruiz et al., 2014; Veedu & Barbot, 2016). Various mechanisms have been proposed for SSEs, such as the fluid overpressure (Kodaira et al., 2004; Liu & Rice, 2007), the friction transitions of rocks from velocity-weakening (VW) to velocity-strengthening (VS) behavior at high slip speeds (Kato, 2003; Liu & Rice, 2005; Shibazaki & Shimamoto, 2007), the dilatancy strengthening of fault gouge (Segall & Bradley, 2012), and the geologic heterogeneity of fault zone (Lavier et al., 2021; Luo & Ampuero, 2018; Skarbek et al., 2012; Wei et al., 2013). In addition, SSEs may play an important role during the earthquake cycle in that they accommodate a significant fraction of a fault's slip deficit and partly release the stress accumulated on the fault. Yet it is worth nothing that some SSEs are followed by huge earthquakes. For example, the 2011 Mw 9.0 Tohoku-Oki earthquake (Kato et al., 2012) and the 2014 Iquique Mw 8.1 earthquake (Kato & Nakagawa, 2014; Ruiz et al., 2014) are preceded by SSEs that migrate toward the hypocenter. In addition, the 2004 Mw 6 Parkfield earthquake is suggested to be preceded by SSEs, about 16 km below the hypocenter (Shelly, 2009). In this context, SSEs are closely related to the nucleation of earthquakes. These observations led to the speculation that SSEs are one of the precursors to earthquakes.

While these investigations significantly expand our understanding of SSEs, it is a great challenge to forecast an impending earthquake based on the monitoring of SSEs, partially because the relationship between SSEs and regular earthquakes (REs) is highly complicated. Some huge earthquakes have been confirmed to be triggered by SSEs. The 2014 Mw 7.3 Papanoa earthquake, for example, was triggered by a slow slip that transfers stress to the hypocenter of the mainshock (Radiguet et al., 2016). Such a triggering mechanism has also been reported for the 2011 Tohoku earthquake (Yokota & Koketsu, 2015) and the 2004 Mw 6 Parkfield earthquake (Khoshmanesh & Shirzaei, 2018). In addition, the occurrence of periodic SSEs in megathrust zone earthquakes in northeastern Japan often coincides with or precedes large earthquakes, indicating a potential triggering mechanism associated with periodic stress perturbations (Uchida et al., 2016). In stark contrast, some SSEs are believed to inhibit huge earthquakes. As SSEs partially release the accumulated stress, the source area of SSEs can act as a barrier to the rupture of major earthquakes nearby (Dixon et al., 2014; Rolandone et al., 2018). On the other hand, SSEs can postpone the next large earthquake because the accumulated slip deficit in the seismic gap might be reduced after SSEs (Radiguet et al., 2012). Besides, SSEs may be not the prerequisite for the nucleation of megathrust earthquakes (Voss et al., 2018) and isolated SSEs might occur as well. Since it is difficult to distinguish the precursory SSEs from regular SSEs (Dong & Xia, 2022), forecasting an impending earthquake based on SSEs observation maybe thus unavailable. Therefore, the study of the interactions between SSEs and REs as well as the underlying mechanism is of great importance to earthquake prediction and hazard mitigation.

Many efforts have been made to resolve the definite relationship between SSEs and REs. The changes in the recurrent patterns of SSEs before an impending earthquake have been reported in numerical simulation in the framework of the rate- and state-dependent friction (RSF) law. For instance, it was found that the recurrence interval of SSEs gradually becomes shorter as the final mainshock is approaching (Matsuzawa et al., 2010; Shibazaki & Shimamoto, 2007). This shortening in recurrence intervals is attributed to the gradual acceleration of slip near the transition zone, implying that the irregular SSEs during the later stage of seismic cycles are a byproduct of the earthquake nucleation process. Importantly, these changes in recurrence patterns may indicate an upcoming huge earthquake, which might help forecast the main earthquakes (Obara & Kato, 2016). Such shorting in the recurrence intervals of SSEs as a larger earthquake is impending has been confirmed in field observations. For example, the evident reduction in recurrence intervals has been documented for the Boso SSEs before the 2011 Tohoku-Oki earthquake (Ozawa, 2014).

Apart from the shorting in the recurrence, other changes in SSEs before the final earthquake are also reported. For instance, it has been proposed that the peak slip velocity of SSEs dramatically increases before the earthquake (Shibazaki & Shimamoto, 2007). In contrast, Luo and Liu (2019) show that the peak slip velocity of SSEs significantly decreases before the megathrust earthquakes. Furthermore, the source region of SSEs may gradually shrink and move down-dip as a huge earthquake is coming (Luo & Liu, 2019). On the other hand, Segall and Bradley (2012) simulated the SSEs and earthquakes on a fault governed by rate-state friction incor-

porating dilatancy and coupled pore-fluid and heat transport. They found that, depending on the size of the low effective-stress VW zone, SSEs may penetrate the locked zone to initiate earthquakes by thermal pressurization or directly evolve into dynamic ruptures. However, the ultimate SSE igniting the dynamic rupture proceeds as the preceding regular SSEs, which is in sharp contrast to the findings aforementioned. Therefore, whether the changes in SSEs are indicative of the upcoming huge earthquake is still in debate.

This study aims to understand the effect of SSEs on the earthquake initiation process. We construct a numerical model to simulate both SSEs and earthquakes during the whole seismic cycle. In the model, faults are governed by the RSF law. Locally increased fluid pressure is assigned on a local patch on the fault, leading to the nonuniformity of effective normal stress. High fluid content and pore pressure are not uncommon for natural faults and have been inferred from the anomalies in seismic velocity (Kodaira et al., 2004) and electrical resistivity (Saffer, 2017), Besides, increased pore pressure has been invoked to explain the occurrence of SSEs (Liu & Rice, 2005). Through systematic parameters studies, we identify four types of fault slip behaviors characterized by SSEs and earthquake initiation modes. Based on the analysis of the stress building up process, we explore the interaction between the SSEs and REs. We also obtain the spectrum of fault slip behaviors, as a function of the parameters of the fluid patch. Afterward, we discuss the effect of SSEs on the nucleation mode and the recurrence interval of earthquakes. Finally, we explore how the monitoring of SSEs can help map the locked fault zone and evaluate seismic potential. Although the findings of this study are merely under a simple model, the fundamental rules that SSEs and earthquakes follow may further our understanding of the mechanism of earthquake initiation and the role of SSEs during seismic cycles.

2. Numerical Model

2.1. Friction Law

We consider a fault governed by the RSF law that is derived from laboratory rock friction experiments (Dieterich, 1979; Ruina, 1983). The shear stress τ on the fault is a function of slip rate V, the state variable θ, and the effective normal stress $\overline{\sigma}$

$$\tau(V, \theta) = \overline{\sigma} \left[\mu_0 + a \ln \frac{V(t)}{V^*} + b \frac{V^* \theta(t)}{D_c} \right] \tag{1}$$

where μ_0 and V^* are the reference friction coefficient and slip velocity, respectively. a and b are nondimensional frictional constants that describe the direct effect and the evolution effect of velocity change, respectively. D_c is the characteristic slip distance that can be interpreted as the distance needed to renew the fault contact state θ. In this study, we adopt Dieterich's "aging-law" (Dieterich, 1979) to describe the evolution of the state variable:

$$\dot{\theta} = 1 - \frac{V(t) \theta(t)}{D_c} \tag{2}$$

This law can account for the healing of faults observed in the laboratory. Assuming that the state variable has evolved into a steady state following a step change in slip velocity, the term on the right in Equation 2 is equal to zero. Then, the state variable at the steady state is D_c/V. Thus, the shear stress at the steady state τ_{ss} is a function of velocity:

$$\tau_{ss}(V) = \overline{\sigma} \left[\mu_0 + (a - b) \ln \frac{V}{V^*} \right] \tag{3}$$

From Equation 3, it can be seen that when $a - b > 0$, the steady shear stress τ_{ss} increases with the increase in slip rate, and thus the fault is VS. Conversely, when $a - b < 0$, the fault is VW (Scholz, 1998). Previous studies have shown that a VS fault always slides stably while a VW fault is conditional stable (Scholz, 1998). A VW fault can develop instabilities once its length exceeds the theoretical critical nucleation zone size L_c (Rice, 1993):

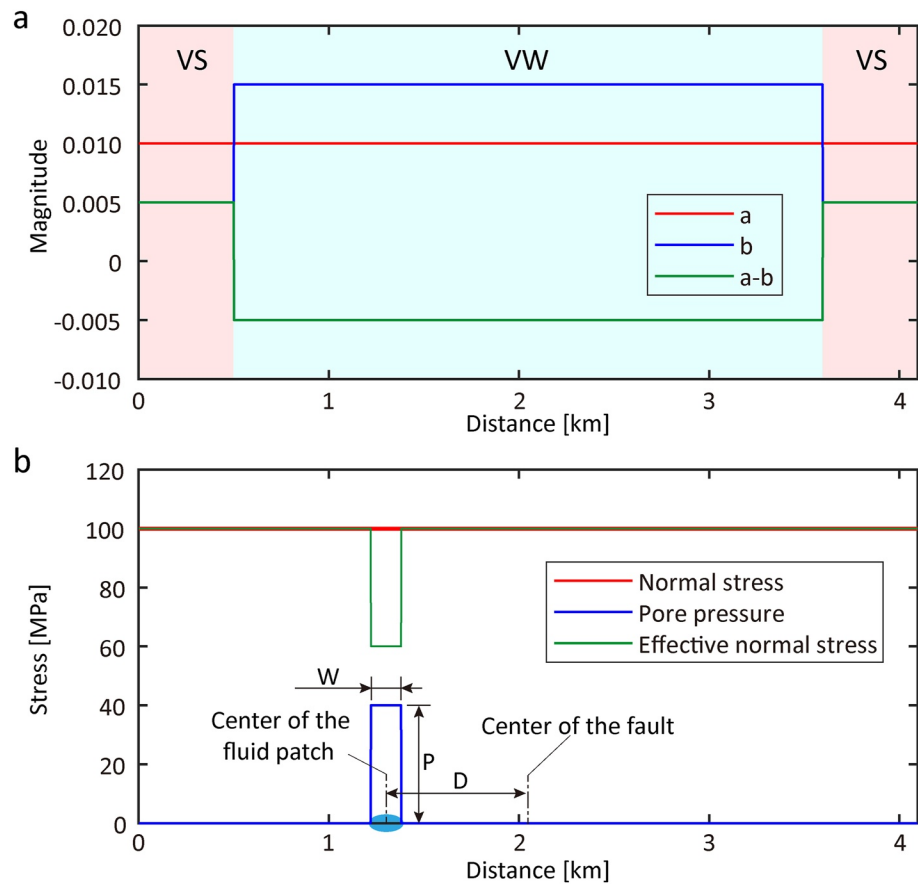$$L_c = C \frac{G D_c}{\overline{\sigma}(b - a)} \tag{4}$$

Figure 1. Friction parameters and stress conditions along the fault. (a) The assigned distribution of the friction parameter $(a - b)$ with $a = 0.010$ and $b = 0.015$ in the central velocity-weakening (VW) segment and $a = 0.010$ and $b = 0.005$ in the velocity-strengthening (VS) segments. (b) Scheme of stress conditions on the fault. The normal stress is homogeneous ($\sigma = 100$ MPa). A fluid patch with increased pore pressure (P) has a width of W. D is the distance between the centers of the fluid patch and the fault.

where G and C are the shear modulus of the crust and the geometry coefficient, respectively. The estimated L_c is derived based on the stability analysis of the fault. There are also several other versions of the estimation of L_c, depending on the competition between a and b (Dieterich, 1992; Rubin & Ampuero, 2005).

2.2. Fault Model

In our model, a 1-D fault is embedded in a 2-D antiplane (mode III) elastic space. The simulated fault model is shown in Figure 1. The fault with a length of $L = 4,096$ m is divided into three segments, with a central VW segment (3,596 m in length) surrounded by two VS segments (250 m in length) with a constant plate rate $V_{pl} = 0.032$ m/y. The distribution of the frictional parameters, that is, a and b, along the fault is shown in Figure 1. Other parameters except effective normal stress are uniform on the fault (i.e., $\mu_0 = 0.6$, $D_c = 0.01$ m, $V^* = 1 \times 10^{-6}$ m/s, and $G = 30$ GPa). These parameter values are not meant to be actual values for natural faults. The stress conditions along the fault are shown in Figure 1b. The normal stress is uniform along the fault ($\sigma = 100$ MPa). Following Equation 4, the settings of the parameter imply $L_c \approx 0.6$ km.

A fluid patch with increased pore pressure (P) is included on the fault. In this work, pore pressure is in the range of 10–90 MPa. We note that the 90 MPa pore pressure is extremely high, almost near-lithostatic. Such near-lithostatic pore pressure has been proposed as the explanation for abnormally high Poisson's ratio, seismic velocity ratio, and electrical resistivity at plate boundaries (Audet et al., 2009; Kodaira et al., 2004; Saffer, 2017; Shelly et al., 2006). Recently, Yao and Yang (2020) have proposed that the strength of the Nicoya megathrust is as

low as 7.5 MPa, which is another evidence for near-lithostatic pore pressure. Thus, the range of pore pressure may cover most cases of real faults. The fluid patch has a width of W, and the distance between the patch center and fault center is D. The existence of the fluid patch leads to heterogeneity in the effective normal stress. Numerical simulations have shown that near-lithostatic pore pressure is one of the possible mechanisms for the occurrence of SSE (Li & Liu, 2017; Liu & Rice, 2005, 2007; Shibazaki et al., 2019). The inhomogeneity of effective normal stress has also been shown to affect the rupture nucleation and propagation (Weng et al., 2015; Yang et al., 2012). In this study, SSEs can be generated by including a small patch with elevated fluid pressure to the central VW segment, as shown in Figure 1b. We investigate the effect of the small fluid patch on the behaviors of SSEs and the nucleation of earthquakes.

2.3. Numerical Simulation Procedure

To perform numerical simulation using the boundary integral equation method, the fault is discretized into $N = 2,048$ subfaults. The discretized cell is thus 2 m in length ($\sim 1/300$ L_c), which is fine enough to resolve the process zone (Rubin & Ampuero, 2009). We use the quasi-dynamic method to simulate the fault slip behaviors. The quasi-dynamic relation between fault slip and shear stress is:

$$\tau_i(t) = -\sum_{j=1}^{N} K_{ij}(u_j(t) - V_{pl}t) - \eta V_i(t) \tag{5}$$

where τ_i and V_i are the shear stress and slip velocity on the ith subfault, respectively. u_j is the slip on the jth subfault. K_{ij} is the elastostatic kernel that relates the slip on the jth subfault to the change in shear stress on the ith subfault. ηV_i is the radiation damping term introduced by Rice (1993) to prevent the unbounded increase of slip velocity during the rupture process. Combining Equations 1, 2, and 5, we get the differential equations governing the fault slip behaviors. These equations are solved using a fourth-order adaptive Runge-Kutta algorithm, where the step doubling technique is used to determine the stepsize (Presse et al., 1992). Besides, the term $\sum_{j=1}^{N} K_{ij}(u_j(t) - V_{pl}t)$ in Equation 5 can be calculated using fast Fourier transform methods, due to the translational invariance of K_{ij}. This method can significantly reduce the computation time from scaling with N^2 to with $N \log_2 N$, which facilitates plenty of simulations under various conditions.

2.4. The Reference Model Without Fluid Pressure

We first present the simulation results of the stress-homogeneous model without fluid pressure for reference. Figures 2a and 2b show the long-term evolution of the slip rate and the friction along the fault, respectively. In Figure 2a, the horizontal axis is the time, and the vertical axis is the fault position. The onset of an earthquake is defined as the moment when the peak slip rate exceeds a threshold of 10^{-3} m/s (V_{seis}). The visual abrupt change in color along the fault represents the occurrence of an earthquake. It can be seen that earthquakes periodically occur on the fault, with a recurrence interval of about 40 yr. During the interseismic stage, two stable creeping zones occupy the VS segments, with a slip rate roughly equal to V_{pl}. The creeping zones gradually penetrate the central VW segment, which is firmly locked with a slip rate on the order of 10^{-14} m/s. The expansion of the creeping zone brings about stress concentration that migrates synchronously with the creeping front (Figure 2b). Meanwhile, shear stress gradually accumulates on the fault (Figure 2c). At the end of the interseismic stage, the two stable creeping zones coalesce (Figure 2a), promoting the slip rate of the entire fault above the background level (i.e., the plate loading rate). An earthquake nucleates later at the center of the VW segment, and then the fault ruptures dynamically. In the coseismic stage, the maximum slip rate V_{peak} could exceed 1 m/s (Figure 2c). At the same time, the stress accumulated during the interseismic stage was drastically released (Figure 2c). When the earthquake ceases, the VW segment locks again, while the VS segments still accommodate plate loading. Afterward, a new seismic cycle starts. This periodical fault activation is similar to the results in previous studies (Barbot, 2019; Wu & Chen, 2014), indicating that our simulation works well.

Figure 2d displays the detailed nucleation process of the earthquake. In the nucleation phase, the nucleation zone with large slip rate expands slowly. At the end of the nucleation phase, the nucleation zone reaches a critical size for instability, which is close to the magnitude of L_c defined in Equation 4. This observation is consistent with experimental observations (Latour et al., 2013; Nielsen et al., 2010; Ohnaka & Kuwahara, 1990) and other classical numerical simulations (Kaneko & Ampuero, 2011; Rubin & Ampuero, 2005). It should also be noted that
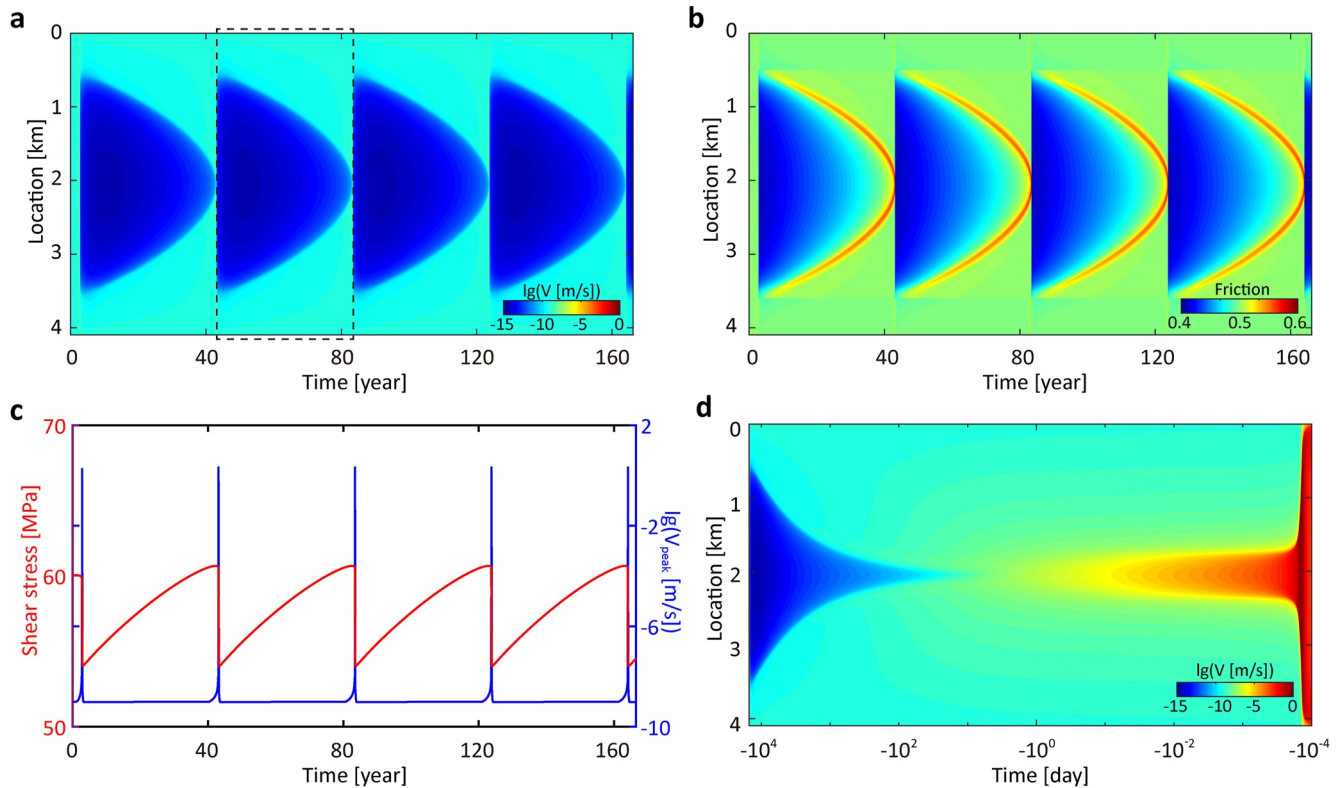
Figure 2. The simulation result for the reference model including none fluid patch. The slip rate (a) and friction (b) along the fault in seismic cycles. (c) The peak slip velocity (V_{peak}) and the average shear stress as a function of time. (d) Slip rate evolution in one seismic cycle corresponding to the dashed box in (a). Note that the time scale in panel (d) is shown in the logarithmic form to display the nucleation process.

in this reference model, no SSEs have been observed during the interseismic stage. Consistently, earthquakes on the stress-homogeneous fault are spontaneously nucleated.

3. Results and Interpretations

3.1. Typical Fault Slip Behaviors: SSEs and Earthquake Nucleation

We perform a total of 300 simulation cases to study the interactions between SSEs and REs. In each simulation case, the total calculation step is set as 100,000. In this way, we have at least six seismic cycles for each case. Since the fault slip in the first earthquake is highly affected by the initial conditions, the results of the first earthquake are out of consideration.

In this work, we define the fault slip with the peak slip rate V_{peak} exceeding V_{seis} (= 10^{-3} m/s) as REs. SSEs are fault slip with $V_{seis} > V_{peak} > 2 V_{pl}$. The fault slip with V_{peak} below $2 V_{pl}$ is considered as fault creeping. Following these criteria, we identify four types of fault slip behaviors in our parameter studies: (a) spontaneously nucleated REs without SSEs, (b) SSEs and spontaneously nucleated REs, (c) SSEs trigger the nucleation of REs, (d) SSEs directly grow into REs. The detailed slip behavior of each type is presented as follows.

3.1.1. Type I: Spontaneously Nucleated REs Without SSEs

Figure 3 shows a typical case of type I, where no SSEs occur during the interseismic stage and the RE initiates spontaneously. The fluid patch with a pore pressure of 40 MPa has a width of 0.4 km (Figure 3a) and its center locates at 0.8 km (point A in Figure 3b). As shown in Figure 3b, the evolution of the slip rate along the fault is very similar to that of the reference model except that the creeping front expends marginally faster in the patch from time T1 to T2. Afterward, this patch persistently slips stably (creep) until the onset of the earthquake (Figures 3c and 3d). The earthquake is nucleated near the center of the fault (point B in Figure 3b, location ≈ 2.09 km) that locked during the entire interseismic stage (Figures 3e and 3f). The detailed nucleation process is shown in
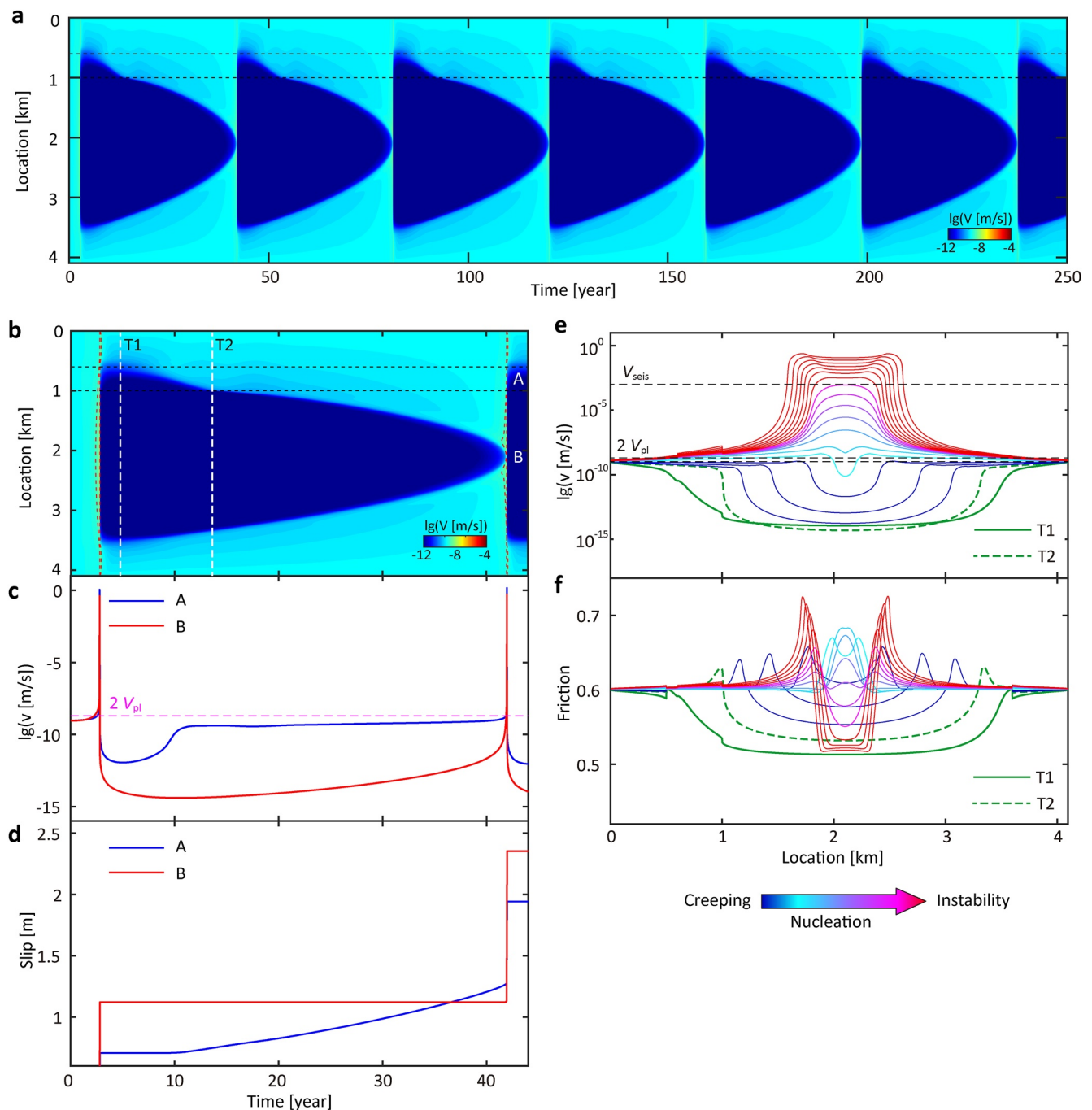
Figure 3. Fault slip behaviors of type I. (a) Fault slip rate in seismic cycles in a model with $P = 40$ MPa, $W = 0.4$ km. The horizontal dashed lines mark the domain of the fluid patch. (b) Detailed fault slip rate in a seismic cycle. A and B correspond to the center of the fluid patch and the fault, respectively. Vertical dashed lines correspond to the moment when the creeping front reaches (T1) and leaves (T2) the fluid patch. (c) The slip velocity at points A and B as a function of time. (d) The cumulative slip at points A and B as a function of time. (e) Snapshots of slip rates from creeping to earthquake nucleation. The results of every 100th step are shown. Also highlighted is the slip rate at times T1 and T2. (f) Snapshots of friction profile from creeping to earthquake nucleation. The results of every 100th step are shown. Also highlighted is the friction at times T1 and T2.

Figure 3e. It can be seen that the nucleation process is almost the same as those on faults without fluid pressure (Fang et al., 2010; Rubin & Ampuero, 2005). Comparing the friction evolution on the right and left portions (Figure 3f), we find that the existence of the fluid patch hardly affects the stress evolution during the interseismic stage, especially in the later stage. This indicates that the stress accumulating process is essentially not disturbed. Therefore, it appears that the earthquake is spontaneously nucleated in its own way.

No evident SSEs are observed in this case, although it has been generally accepted that increased fluid pressure could generate SSEs (Kodaira et al., 2004; Liu & Rice, 2007). We speculate that the absence of SSEs in this study is due to the adjacency between the fluid patch and the VS segment outside. Since the stable creeping VS segment can be considered as a barrier to rupture (Kaneko et al., 2010; Perfettini et al., 2010), it may prevent the increase in slip rate at the patch. Therefore, SSEs are prohibited in this model. The irrelevant pattern between the fluid patch and the earthquake may be due to the large interval between the patch (center at point A) and the nucleation zone (center at point B). When the patch undergoes creeping in the early interseismic stage, the final nucleation zone is still firmly locked. It takes about 30 yr for the creeping front to travel from point A to point B. Therefore, the accumulation of long-term tectonic loading plays a dominating role in generating the earthquake.

3.1.2. Type II: SSEs and Spontaneously Nucleated REs

Figure 4 presents a typical case of type II, where SSEs episodically occur during the interseismic stage and the RE initiates spontaneously. In this case, the fluid patch with pore pressure of 80 MPa has a width of 0.16 km (Figure 4a) and its center locates at 1.3 km (point A in Figure 4b). As shown in Figure 4b, in the interseismic stage, the slowly expanding fault creeping is interrupted by two SSEs successively. The first SSE develops when the creeping front reaches the edge of the patch. Both SSEs initiate near the edge of the patch and propagate bilaterally at a velocity of 1~2 km/yr, about two orders of magnitude higher than the expanding velocity of the creeping front. The second SSE is more energetic and featured with a higher slip rate, higher slip, larger source area, and longer source duration than the first one (Figures 4b–4d). This increase in slip rate within the sequence of SSEs is generally consistent with previous observations (F. Hirose & Maeda, 2013; Shibazaki & Shimamoto, 2007), although the model setup and friction law are not identical. After the quenching of the SSEs, the slip rate in the source zone of the SSEs drops slightly below the background level. The occurrence of SSEs hastens the expansion of the creeping zone and the shrinkage of the locked zone. Finally, an earthquake is nucleated at point B (location ≈ 2.15 km) about 5 yr after the second SSE. Figure 4e presents the nucleation process of the earthquake. In the beginning, there are two nucleation zones: a small nucleation zone at the patch and a large nucleation zone at the center of the fault. Afterward, the larger nucleation zone expands while the small nucleation zone keeps its size unchanged. Eventually, the earthquake bursts from the large nucleation zone and merges the small nucleation zone in the dynamic rupture process. The seismic cycle is about 39.65 yr, smaller than that of the reference model.

We examine the relationship between the SSEs and the final RE based on the stress evolution process. The friction distribution during the nucleation process, and before and after the SSEs, is shown in Figure 4f. The SSEs release a fraction of stress on its source zone and transfer stress to the center of the fault. Although the second SSE brings about a non-negligible stress increase in the final nucleation zone, the nucleation zone is still locked ($V \approx 10^{-12}$ m/s, as shown in Figure 4e) and no earthquakes occur until 5 yr later. Therefore, the SSEs proceed as separate events followed by no mega earthquakes, as are the SSEs extensively observed in the subduction zones worldwide (Avouac, 2015; Rogers & Dragert, 2003). Besides, it has been proposed that SSEs are not necessarily related to the immediate occurrence of the giant earthquake, because it is insufficient to demonstrate causality (Graham et al., 2014; Ohtani et al., 2014; Voss et al., 2018). Therefore, we would approve that, in those cases, the earthquakes are nucleated spontaneously rather than triggered by SSEs. Nevertheless, it should be noted that the occurrence of SSEs could temporarily accelerate the propagation creeping front, which may bring the RE forward.

3.1.3. Type III: SSEs Trigger the Nucleation of REs

Figure 5 presents a typical case of type III, in which SSEs trigger the nucleation of REs. In this case, the fluid patch with pore pressure of 40 MPa has a width of 0.16 km and its center locates at 1.3 km (point A in Figure 5b). In a seismic cycle (Figure 5b), we observe two SSEs during the interseismic stage. The first SSE begins about 10 yr before the final earthquake and lasts no more than 2 yr. Three years before the final earthquake, the second SSE initiates near the edge of the patch (point A) with pore pressure and expands bilaterally. Similar to the previous case, the second SSE is more energetic than the first one (Figures 5c and 5d). What is striking about the second SSE is that the SSE skips the locked central fault segment (Figure 5b) and emerges on the other side of the fault (point C in Figures 5b–5d). The second SSEs encircles the firmly locked fault segment. It looks that the locked zone behaves as a barrier to SSEs, prohibiting the consecutive propagation of SSEs along the fault. Subsequently, the second SSE persistently propagates toward the center of the locked segment (point B, location ≈ 2.06 km),
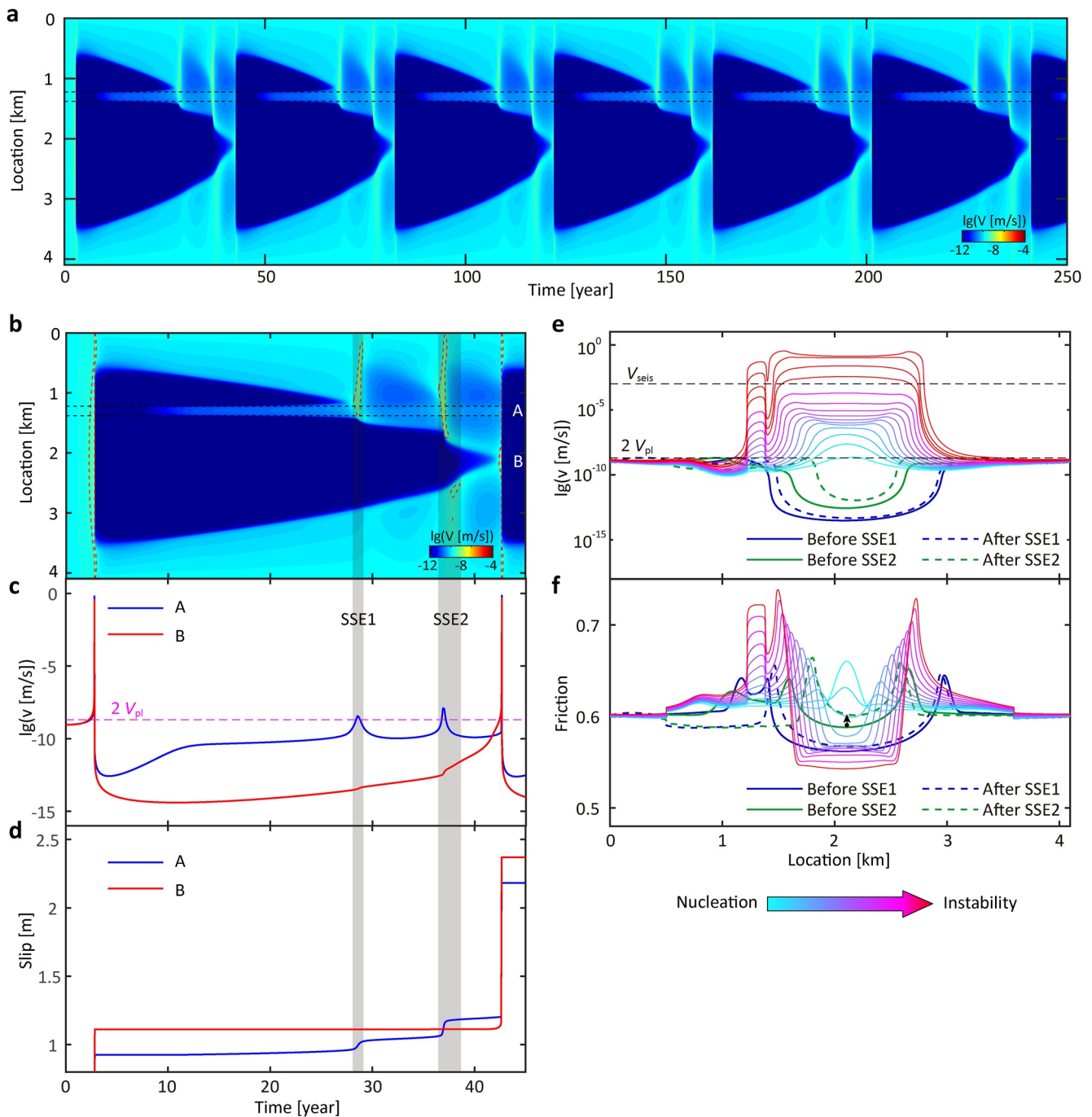
Figure 4. Fault slip behaviors of type II. (a) Fault slip rate in seismic cycles in a model with $P = 80$ MPa, $W = 0.16$ km. The horizontal dashed lines mark the domain of the fluid patch. (b) Detailed fault slip rate in a seismic cycle. A and B correspond to the center of the fluid patch and the fault, respectively. The red contour corresponds to the slip rate of $2 V_{pl}$. (c) The slip rate at A and B as a function of time. (d) The cumulative slip at A and B as a function of time. (e) Snapshots of slip rates during the earthquake nucleation phase. Every 100th step is shown. Also highlighted is the slip rate before and after the slow slip events (SSEs). (f) Snapshots of friction during the earthquake nucleation phase. Every 100th step is shown. Also highlighted is the friction before and after the SSEs. The dashed arrow indicates the stress building up at the nucleation zone during the period of the second SSE.

pushing the slip rate at the locked segment above the background level (Figure 5e). Ultimately, the second SSE erases the locked segment and leads up to the nucleation of the final earthquake.

The triggering mechanism, in this case, is explored based on the analysis of stress evolution. By comparing the friction distribution before and after the second SSE (Figure 5f), we find that the second SSE significantly change
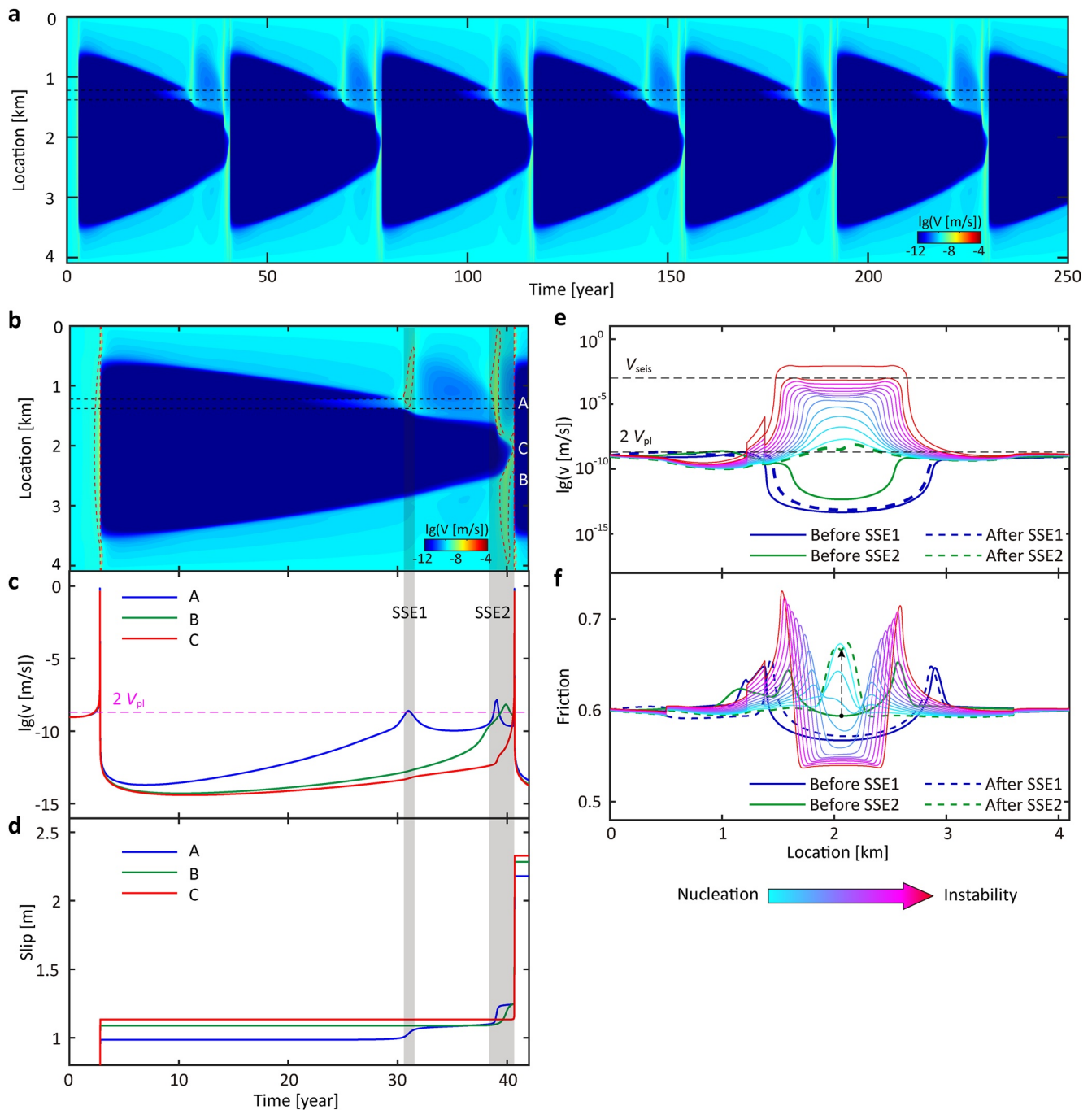
Figure 5. Fault slip behaviors of type III. (a) Fault slip rate in seismic cycles in a model with $P = 40$ MPa, $W = 0.16$ km. The horizontal dashed lines mark the domain of the fluid patch. (b) Detailed fault slip rate in a seismic cycle. A–C correspond to the fluid patch center, the point at 2.7 km, and the fault center, respectively. The red contour corresponds to the slip rate of $2 V_{pl}$. (c) The slip rate at A–C as a function of time. (d) The cumulative slip at A–C as a function of time. (e) Snapshots of slip rates during the earthquake nucleation phase. Every 100th step is shown. Also highlighted is the slip rate before and after the slow slip events (SSEs). (f) Snapshots of friction during the earthquake nucleation phase. Every 100th step is shown. Also highlighted is the friction before and after the SSEs. The dashed arrow indicates the stress building up at the nucleation zone during the period of the second SSE.

the stress distribution in that it transfers stress to the locked segment. After the second SSE, there is a sharp increase in friction at the center of the locked segment, where the earthquake nucleation starts before long. Thus, the final earthquake nucleation is likely to be triggered by the shear stress concentration induced by the second SSE. Recently, Saltogianni et al. (2021) reported that two SSEs precede the 2018 Mw 6.9 Zakynthos earthquake. The first SSE in 2014 generated mild Coulomb stress changes (≤ 3 kPa) and thus did not trigger the final event,

while the second SSE in 2018 caused stress changes up to 25 kPa, ultimately triggering the earthquake. This observation is qualitatively similar to our numerical case. Besides, the scenario that earthquakes triggered by SSEs has been confirmed by field observations (Kato et al., 2012; Radiguet et al., 2016; Yokota & Koketsu, 2015) and other numerical studies (Segall & Bradley, 2012).

3.1.4. Type IV: SSEs Directly Evolve Into REs

Figure 6 presents a typical case of type IV, in which SSEs directly evolve into RE. In this case, the fluid patch with pore pressure of 80 MPa has a width of 0.44 km and its center locates at 1.3 km (point A in Figure 6b). As shown in Figure 6b, in the early interseismic stage, local creep has already developed on the patch about 20 yr before the arrival of the creeping front that propagates inward (Figure 6b). We observe three SSEs during the interseismic stage (Figures 6b–6d). The first and the second SSE initiate near the edge of the patch about 16 and 8 yr before the final earthquake, respectively. About 1 yr before the final earthquake, the last SSE occurs and encircles the central fault segment (point B, location ≈ 2.91 km) that is firmly locked, culminating in a final earthquake. Figure 6e explicitly shows the slip rate distribution during the initiation process of the earthquake. Depart from the previous cases where the final earthquakes are always nucleated near the center of the fault, in this case, the earthquake initiates on the right side of the fault, where the third SSE is ongoing. Furthermore, when the earthquake has launched, the central segment of the fault is still locked, without attaining a slip rate around the background level. It appears that the locked segment serves as a barrier to the earthquake rupture at the outset.

Figure 6f shows the stress evolution along the fault. The first and second SSEs slightly change the stress distribution, as is the case of type II. Although the third SSE transfers considerable stress to the central locked segment, it does not trigger the nucleation of the earthquake there. The evolution of stress along the fault implies that the SSE on the right side has occurred in the nucleation zone of the impending earthquake. This is similar to what was documented for the 2014 Mw 7.8 Iquique Mw 8.1 earthquake (Ruiz et al., 2014). It should be noted that the SSE leads to no increase in shear stress in the nucleation zone of the final earthquake. Therefore, it is not likely that the final earthquake is triggered by the SSE. We argue that the third SSE itself evolves into the final earthquake since the third SSE is exactly the nucleation of the final earthquake. This is similar to previous studies (Ohtani et al., 2019; Segall & Bradley, 2012) and the nucleation mechanism is better resolved in this study. Field observation has reported that the 2012 Mw 7.6 earthquake in Costa Rica are preceded by SSEs and the Coulomb stress change caused by the SSE at the hypocenter is supposed to be too small to trigger the mainshock (Voss et al., 2018). Our numerical result explicitly provides a possible mechanism for the occurrence of this earthquake.

3.2. Spectrum of Fault Slip Behaviors

To evaluate the dependence of the four types of fault slip behaviors on the parameters of the fluid patch (i.e., pore pressure, patch location, and patch size), we inspect all the simulation results in this study. The combined effects of pore pressure, patch size, and patch location is shown in Figure 7. If the fluid patch is located at the center or near the edge of the VW segment, there are no SSEs. On the other hand, when the fluid patch is off the center of the VW segment, SSEs are frequently observed and the occurrence of SSE is strongly dependent on the fluid pressure and patch size. Generally, the frequency of SSEs tends to increase with fluid pressure and patch size.

In addition, the regime in which earthquakes initiate is controlled by the parameters of the fluid patch. When the fluid patch is located near the edge or at the center of the VW segment, the nucleation of earthquakes follows the scenario of either type I or type II. However, when the fluid patch is off the center, the nucleation of earthquakes is more complex. As shown in Figure 6, higher fluid pressure and larger patch size always favor SSEs to directly grow into REs. On the contrary, decreased fluid pressure and narrow patch facilitate the triggered nucleation of REs. In the residual cases, earthquakes are nucleated spontaneously, without any evident connections with SSEs. Besides, SSEs may shift the possible nucleation location of REs by transferring shear stress further away from the center of the fault.

Furthermore, the earthquake recurrence intervals are influenced by the fluid patch. If the patch is near the edge or at the center of the VW segment, the increase in pore pressure and patch size will result in shortened recurrence intervals. The shortening in recurrence intervals is more prominent when the fluid is at the center, indicating that the edge patch does not play an important role in earthquake cycles, as is the case in Figure 3. On the other hand, if the fluid patch is off the center, the effect of the fluid patch is more complicated. It looks like that the earthquake recurrence intervals are coupled with the SSEs frequency and the earthquake nucleation regime. This
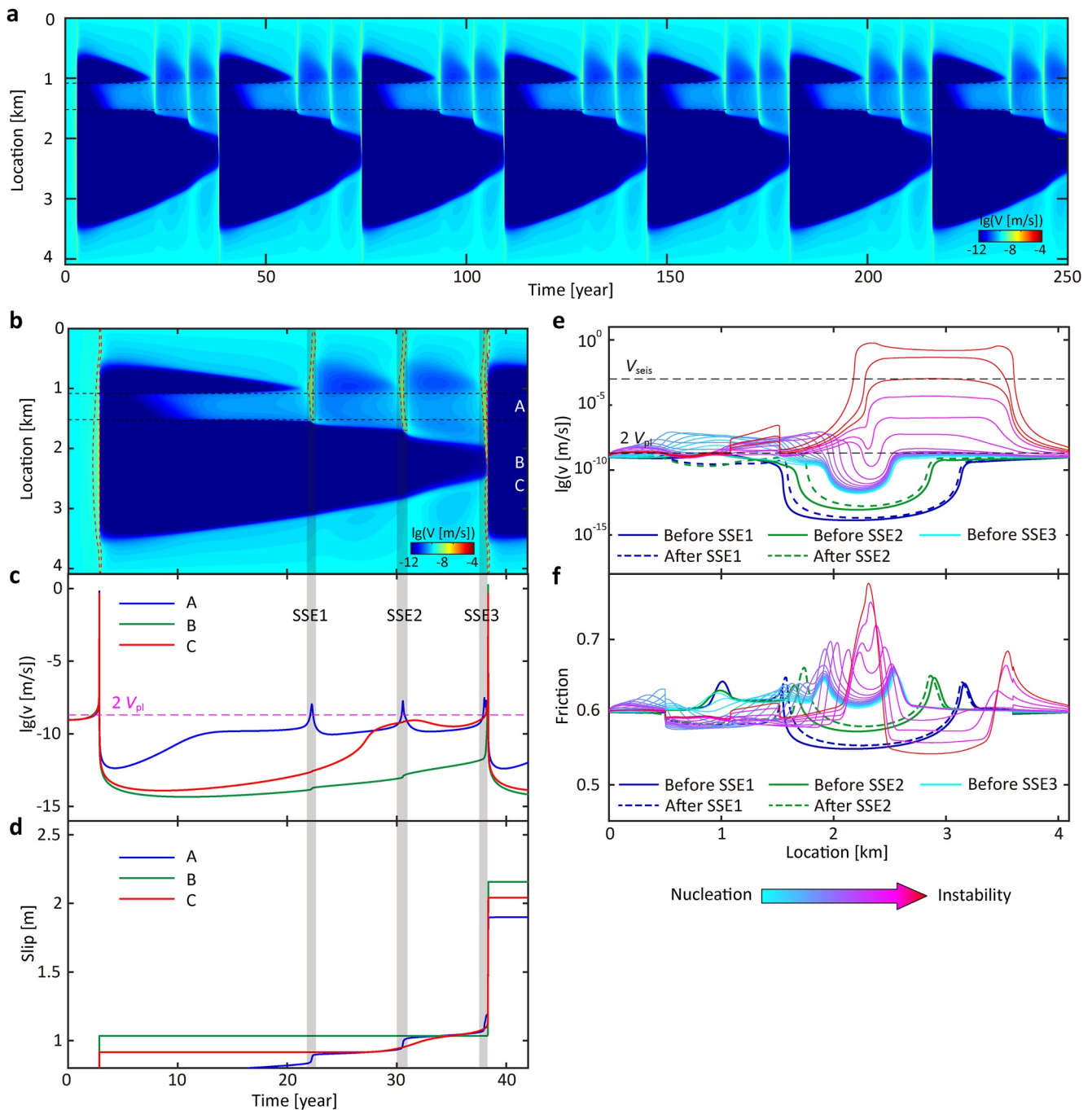
Figure 6. Fault slip behaviors of type IV. (a) Fault slip rate in seismic cycles in a model with $P = 80$ MPa, $W = 0.44$ km. The horizontal dashed lines mark the domain of the fluid patch. (b) Detailed fault slip rate in a seismic cycle. A–C correspond to the fluid patch center, the point at 2.2 km, and the point at 2.9 km, respectively. The red contour corresponds to the slip rate of $2 V_{pl}$. (c) The slip rate at A–C as a function of time. (d) The cumulative slip at A–C as a function of time. (e) Snapshots of slip rates during the earthquake nucleation phase. Every 100th step is shown. Also highlighted is the slip rate before and after the slow slip events (SSEs). (f) Snapshots of friction in the last stage of the seismic cycle. Every 100th step is shown. Also highlighted is the friction before and after the SSEs.

is accessible because the occurrence of earthquakes is closely associated with the nucleation process and the behaviors of SSEs in these cases.

How the localized heterogeneity in stress affects the fault slip or rupture behaviors of the entire fault is one of the intriguing problems relevant to earthquake mechanisms (Yang et al., 2022; Yao & Yang, 2022). The transition in fault slip behaviors and rupture process has been documented in previous studies incorporating fric-
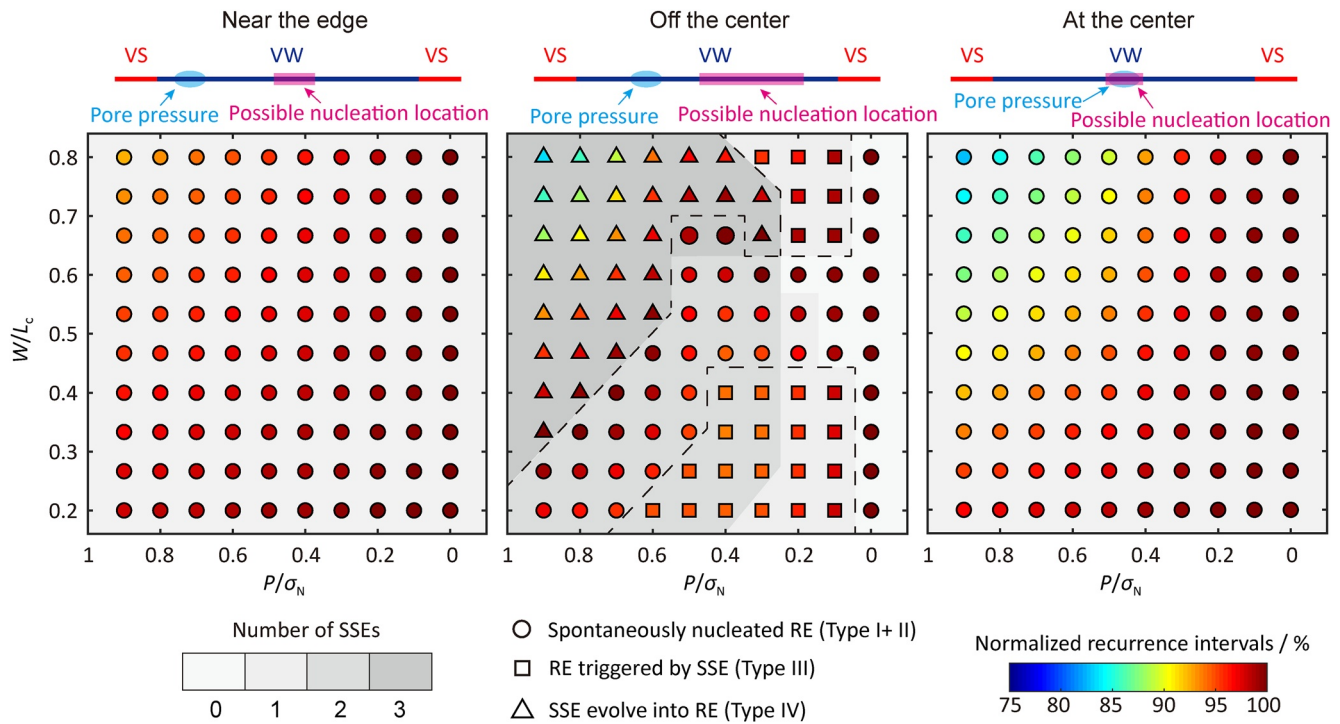
Figure 7. Phase diagram for different types of fault slip behaviors as a function of the location, pore pressure, and the width of the fluid patch. The fault patch is located near the edge (left), off the center (middle), and at the center (right) of the velocity-weakening (VW) segment. Possible nucleation location of regular earthquakes (REs) is represented as magenta strips.

tion heterogeneity (Dublanchet, 2018; Luo & Ampuero, 2018; Skarbek et al., 2012; Yabe & Ide, 2018; Yao & Yang, 2020). In these studies, the selection of fault slip behaviors is mainly controlled by the spatially averaged values of frictional parameters. Some studies suggest that fault slip behaviors depend on the asperities/barriers on the fault (Ariyoshi et al., 2012; Kato, 2004, 2020; Noda et al., 2013; Weng et al., 2015; Yang et al., 2012). The breakage of the asperities and the interactions between them dominate the fault slip behaviors, including slip modes and seismic cycles. In this study, we conduct systematic parameter studies and present the spectrum of slip behaviors of faults with local decreased effective normal stress. Our results validate that the existence of locally increased fluid pressure plays an important role in determining the slip behaviors of the entire fault, which are more complicated than those of faults with uniform stress.

3.3. SSEs Bring the Final REs Forward

Previous studies have shown that the occurrence of SSEs signals a period of increased probability for large earthquakes (Liu & Rice, 2005; Mazzotti & Adams, 2004), while others argued that SSE may delay the occurrence of large earthquakes (Radiguet et al., 2012). In this study, we examine the above points of view by comparing the recurrence interval of the earthquakes preceded by SSEs (T_{rec}) to that of the characteristic earthquakes in the reference model (T_{rec}^{ref}). As shown in Figure 8, if T_{rec} is shorter than T_{rec}^{ref}, the final earthquake is brought forward. The difference between T_{rec}^{ref} and T_{rec} is defined as clock advance. Otherwise, the occurrence of the final earthquake is delayed or not disturbed by SSEs.
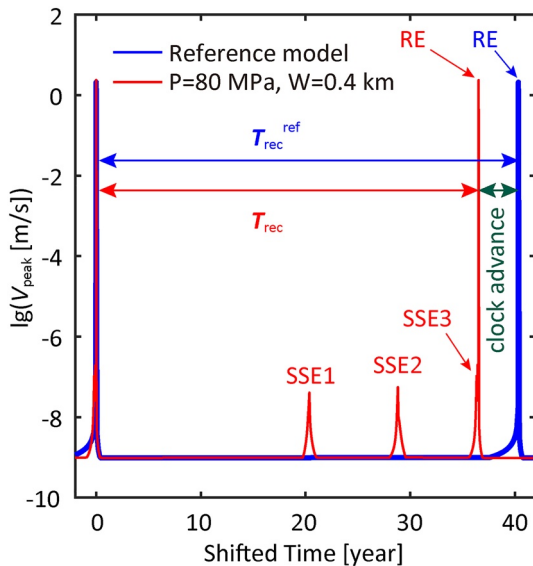

Figure 8. Comparison of the recurrence interval of the earthquakes preceded by slow slip events (SSEs; T_{rec}) and the recurrence interval of the reference model (T_{rec}^{ref}). In this case, the earthquake is brought forward because T_{rec} is shorter than T_{rec}^{ref}. The difference between T_{rec}^{ref} and T_{rec} is defined as clock advance.
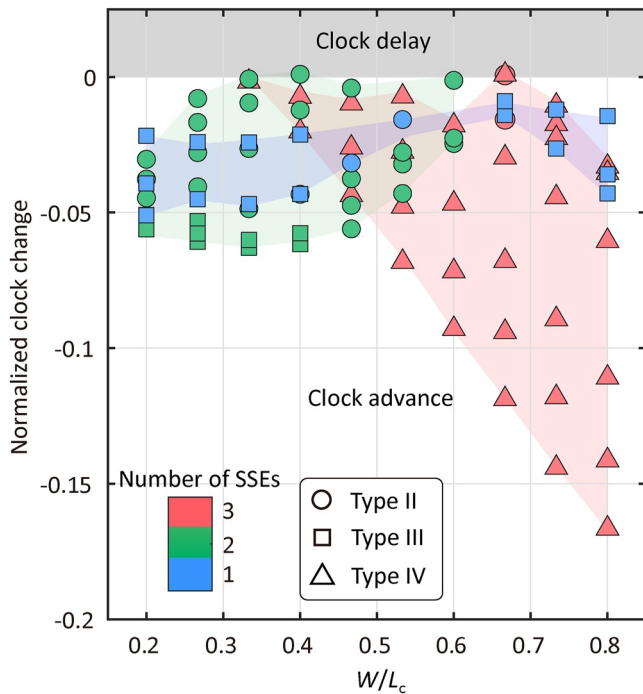
Figure 9. Clock changes of regular earthquakes arise from slow slip events (SSEs). The clock changes are normalized by T_{rec}^{ref} (= 40.33 yr). Negative clock change represents the shortening of the recurrence interval, that is, the final earthquake is brought forward.

Figure 9 collectively presents the clock change of T_{rec} relative to T_{rec}^{ref}. We find that the SSEs virtually advanced the occurrence of the final earthquake. Interestingly, the clock change is affected by the frequency of SSEs during the interseismic stage. The clock advance for cases with only one or two SSEs is usually less than 0.07 T_{rec}^{ref} (~2.8 yr), while the cases with three SSEs have a peak clock advance of about 0.18 T_{rec}^{ref} (~7 yr), which is about one-fifth of the seismic recurrence interval. Moreover, the clock change is related to the earthquake nucleation modes. Intuitively, there is a prominent clock advance for the cases of type IV, where SSEs directly grow into REs. Therefore, our results are against the perspective that SSEs delay the occurrence of large earthquakes (Radiguet et al., 2012). It is true that SSEs release a fraction of the stress in the source area. However, SSEs may drive the entire fault to a more sufficiently stressed state and bring the slip rate above the background level (Figures 4–6). Although the occurrence of SSEs does not necessarily mean the immediate rupture of a large earthquake (Ohtani et al., 2014), there is a temporal acceleration in the preparation process for large earthquakes.

4. Discussion

4.1. Interactions Between SSEs and REs

The interactions between SSEs and REs have been deeply addressed in detail, but no consensuses have been reached (Ohtani et al., 2014; Radiguet et al., 2016; Voss et al., 2018; Yokota & Koketsu, 2015). In this study, we explore the interrelationship between REs and SSEs caused by locally increased fluid pressure. We have observed four types of fault slip behaviors distinguished by SSEs and earthquake initiation process, which are reminiscent of natural earthquakes. For example, earthquakes directly triggered by SSEs are reported for natural earthquakes, such as the 2014 Mw 7.3 Papanoa earthquake (Radiguet et al., 2016), the 2011 Mw 9.0 Tohoku earthquake (Yokota & Koketsu, 2015), and the 2014 Mw 8.1 Chile megathrust earthquake (Socquet et al., 2017). Besides, the observation that SSEs grow into a RE may shed light on the nucleation mechanism of the 2012 Mw 7.6 earthquake in Costa Rica (Voss et al., 2018).

Our results highlight that the interactions between SSEs and REs are conditioned by the characteristics of the fluid patch. Previous numerical studies have produced various SSEs, closely associated with large earthquakes or not (F. Hirose & Maeda, 2013; Li & Liu, 2017; Luo & Liu, 2019; Ohtani et al., 2014; Segall & Bradley, 2012; Shibazaki et al., 2010; Skarbek et al., 2012). In those studies, the occurrence of SSEs may be a combined effect of friction property, fault geometry, and stress condition. Specifically, several innovative studies include the fluid diffusion dynamics during the seismic cycles, providing profound insights into the fluid driven aseismic slip (Liu & Rubin, 2010; Zhu et al., 2020). In this study, only the heterogeneity of effective normal stress is incorporated in the simple fault model. Interestingly, our results still reproduce the diversity of natural fault slip behaviors. Thus, our simulation is also compatible with the perspective that fault heterogeneity in stress conditions could play a crucial role in determining the fault slip behaviors (Luo & Liu, 2021; Yang et al., 2012, 2013; Yang, Yao, He, & Newman, 2019; Yang, Yao, He, Newman, & Weng, 2019). However, it is still challenging to predict fault slip behaviors since the natural fault plane is a mosaic of locked, creeping, and slow slipping patches at a wide variety of length scales, more complex than the numerical models in this study.

One may be concerned about whether the periodic mirror effect resulting from short VS segment could affect the fault slip behaviors as well as the interactions between SSEs and REs. By comparing the long-term fault slip behaviors with two models with different VS segment lengths (Figures S1 and S2 in Supporting Information S1), we confirm that the length of VS segment does not significantly affect the long-term slip behaviors of faults. Thus, in this work, the periodic mirror effect does not modify our results on the first order.
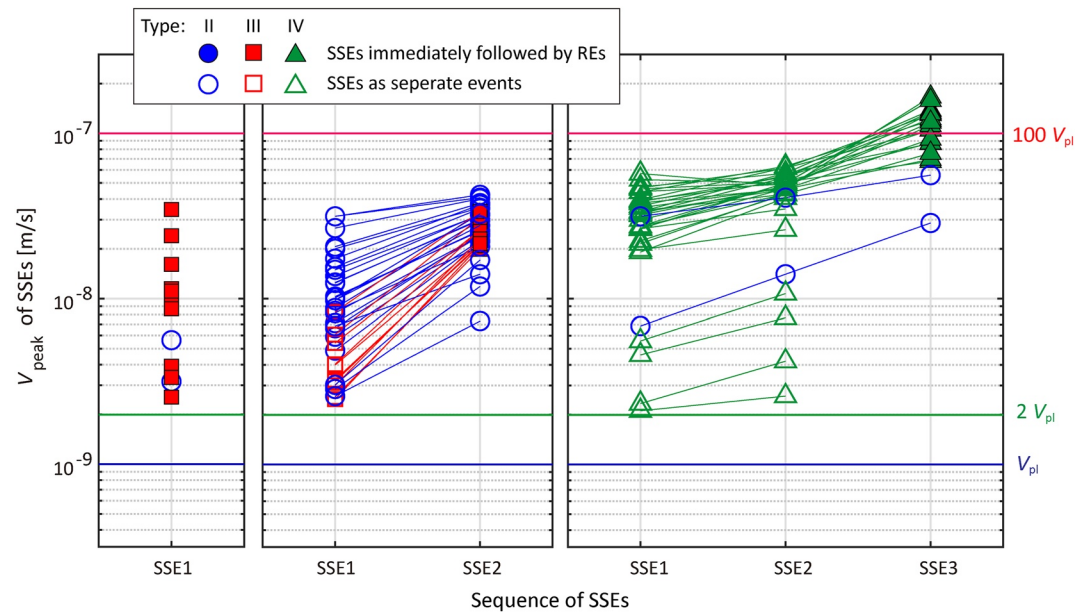
Figure 10. Relationships between the peak slip rate of slow slip events (SSEs) and final earthquakes. The left, middle, and right panels display the cases where one, two, and three SSEs occur during the interseismic stage. SSEs immediately followed by regular earthquakes (REs) are represented as filled cycles, squares, and triangles. SSEs develop as separate events are shown as open symbols. Cycles, squares, and triangles represent the fault slip behaviors of types II, III, and IV, respectively. The symbols connected by lines belong to one seismic cycle.

4.2. Source Area of SSEs Maps Locked Fault Zone

Previous studies have proposed that the highly coupled fault zone or the rupture of the impending earthquakes can be outlined by SSE, because the SSEs partially released the stress in their source area, impeding the rupture propagation of final earthquakes (Dixon et al., 2014; Rolandone et al., 2018). The weak coupling patch always matches the location of SSEs well (Bürgmann, 2018). Our results support this viewpoint. As shown in Figures 5 and 6, the source area of SSEs is not continuous along the fault. The traveling SSEs front usually decelerates or stops upon hitting the edge of the locked zone. The discontinuity in the spatiotemporal distribution of SSEs coincidently matches the locked zone. This implies that SSEs can be considered as an inherent fault gauge that can be used to delineate the locked fault zone. Thus, our result motivates careful and precise monitoring of SSEs that might help predict the possible extent of locked fault zones and constraint earthquake magnitude.

On the other hand, the locked zone is a barrier to the propagation of SSEs, since the locked zone invariably hinders the migration of SSEs along the fault. However, due to the stress transfer induced by SSEs, the locked zone is gradually corroded and driven to failure. This concept has also been used to explain the unfastening of the locked fault zone with the successive migration of SSEs (Uchida et al., 2020).

4.3. Increased Slip Rate of SSEs as a Plausible Precursor of REs?

Recent advances in observation point to that SSEs may prove useful for short-term earthquake forecasts (Voss et al., 2018). However, how to predict the occurrence of large earthquakes based on SSEs remains unclear (Obara & Kato, 2016). Previous studies have shown that the peak slip velocity of SSEs changes as a huge earthquake is approaching (Luo & Liu, 2019; Shibazaki & Shimamoto, 2007). However, these results contradict each other. Here, we explore the possible precursors in the peak slip velocity of SSEs in our studied model.

Figure 10 displays the peak slip velocity (V_{peak}) of each SSE. For the cases with only one SSE during the interseismic stage, it seems that SSEs with a higher V_{peak} have a higher potential to trigger a huge earthquake. However, there is no clear triggering threshold in V_{peak}. If there are two SSEs during the interseismic stage, the V_{peak} of the second SSE is always higher than that of the first SSE, especially for the cases where SSEs trigger earthquakes

(type III). This means that SSEs with $V_{\text{peak}} > 20\,V_{\text{pl}}$ ($\sim 2 \times 10^{-8}$ m/s) are more likely to trigger huge earthquakes. However, for the cases where earthquakes are nucleated spontaneously (type II), SSEs assuming V_{peak} exceeding $20\,V_{\text{pl}}$ still occur as separate events and are not immediately followed by earthquakes. These results suggest that it is difficult to discriminate the SSEs having the potential to trigger huge earthquakes on the basis of the peak slip velocity. For the cases where three SSEs occur during the interseismic stage, the V_{peak} of SSEs increases with the order of SSEs in the sequence. The SSEs with V_{peak} exceeding $70\,V_{\text{pl}}$ ($\sim 7 \times 10^{-8}$ m/s) have the potential to directly grow into huge earthquakes, while others always occur as separate events. There is a clear threshold in V_{peak} for an SSE to transform into a huge earthquake ($V_{\text{peak}}^{\text{thre}} \approx 70\,V_{\text{pl}}$).

Our numerical results are partially consistent with the work of Shibazaki and Shimamoto ([2007](#)), where the V_{peak} of SSEs increases with time during the interseismic period. This may reflect the loosing of the fault as stress continuously builds up in the zone where SSEs occur. However, our results show that it is difficult to infer whether an SSE could trigger a huge earthquake. The SSEs with V_{peak} even slightly higher than the background creeping rate could trigger a huge earthquake. Our results imply that it may be impracticable to decide whether an SSE could trigger huge earthquakes merely based on the magnitude of V_{peak}. On the other hand, SSEs with extremely high V_{peak} are promising to directly transform into huge earthquakes. This finding reminds us that the occurrence of SSEs could lead to an increased possibility of huge earthquakes, which is consistent with previous views (Mazzotti & Adams, [2004](#)). Therefore, the careful and precise monitoring of SSEs is necessary and may allow for improved earthquake hazard assessment.

4.4. Relationships Between the Rupture Length of SSEs and the Occurrence of REs

Although we elucidate the connections between the peak slip rate of SSEs and the occurrence of REs in the above section, the peak velocity of natural SSEs is rather difficult to determine, partially because of the limited resolution of observation and the complicated temporal and spatial evolution of SSEs. For SSEs, the spatial extent may be a source parameter that can be constrained more reliably than V_{peak}. Here, we discuss the relationships between the rupture length of SSEs and the occurrence of REs.

Figure [11](#) presents the rupture length of SSEs (L_{SSE}) in seismic cycles. One can see that L_{SSE} almost increases with the order of SSEs in the interseismic stage, which is in contrast to previous results (Luo & Liu, [2019](#)). One possible explanation is that as the tectonic loading is ongoing, stress is building up on more parts of the fault, facilitating the rupture propagation of SSEs. Almost all L_{SSE} exceed the critical rupture length of nucleation, L_{c}. This suggests that the initiation of dynamic ruptures cannot be simply deduced from the growth of stable rupture, if the conventional earthquake nucleation cannot be distinguished from SSEs. Moreover, some general trends in the rupture length of SSEs may provide useful insights into earthquake hazard assessment. The compilation of L_{SSE} indicates that SSEs immediately followed by earthquakes are usually associated with $L_{\text{SSE}} > 0.44\,L$, while the SSEs developing as separate events are characterized with $L_{\text{SSE}} < 0.76\,L$. Therefore, if $L_{\text{SSE}} > 0.76\,L$, it is likely that an earthquake is approaching. By contrast, if $L_{\text{SSE}} < 0.44\,L$, we may speculate that no earthquakes would happen. When $0.44\,L < L_{\text{SSE}} < 0.76\,L$, it is difficult to determine whether an earthquake will occur. In general, the rupture length of SSEs, to some extent, is correlated with the occurrence of earthquakes.

For natural faults, field observations show that the rupture length of SSEs varies with time, from tens of kilometers to several hundreds of kilometers (Michel et al., [2018](#)). However, to our knowledge, this is no solid evidence to show that SSEs with larger spatial extent have the propensity to promote the initiation of earthquakes. Recently, it is proposed that the coalescence of SSEs may bring the fault closer to failure, leading to the initiation of earthquakes (Bletery & Nocquet, [2020](#)). The coalescence of SSEs represents the pronounced increase in the spatial extent of SSEs. Thus, this scenario may be consistent with our results.

5. Conclusion

In this study, we performed a systematic study to explore the fault slip behaviors during the whole seismic cycle, especially the interactions between SSEs and earthquake initiation. The fault is governed by the RSF law, and SSEs are generated by including locally increased fluid pressure. We identify four types of fault slip behaviors distinguished by SSE and earthquake initiation mode, which are dependent on the localized fluid patch. To summarize, (type I) no SSEs emerge and REs are nucleated spontaneously, (type II) SSEs occur as separate
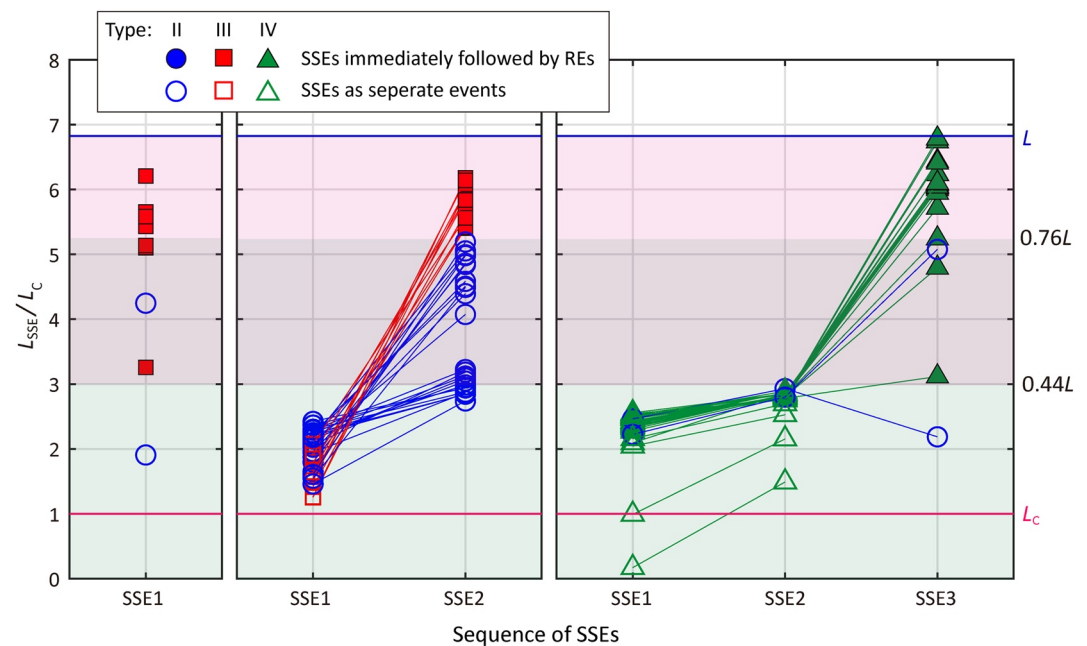
Figure 11. Relationships between the rupture length of slow slip events (SSEs; L_{SSE}) and final earthquakes. The rupture length of SSEs is normalized by L_c. The left, middle, and right panels display the cases where one, two, and three SSEs occur during the interseismic stage. SSEs immediately followed by regular earthquakes (REs) are represented as filled cycles, squares, and triangles. SSEs evolving as separate events are shown as open symbols. Cycles, squares, and triangles represent the fault slip behaviors of types II, III, and IV, respectively. The symbols connected by lines belong to one seismic cycle.

events and REs are nucleated spontaneously, (type III) SSEs trigger the nucleation of REs, and (type IV) SSEs directly grow into REs. The various fault slip behaviors are reminiscences of reported natural earthquakes. The mechanism of the earthquake initiation has been discussed, based on the analysis of the stress evolution process. Our results suggest that heterogeneity in stress plays a crucial role in determining fault slip behaviors, even in such a simple numerical fault model.

Our results reveal that SSEs may lead to a temporary acceleration in fault decoupling. The locked zone always shrinks faster during the period of SSEs. On the other hand, the locked zone behaves as a barrier to traveling SSEs. Therefore, monitoring SSEs can help map the extent of the locked zone and infer the stage within the seismic cycle. In addition, the peak slip velocity of SSEs might be related to the occurrence of huge earthquakes. The possibility of huge earthquakes may increase during the SSEs because SSEs with extremely high peak slip velocity may directly transform into huge earthquakes. However, there is no clear threshold in the peak slip velocity for SSEs to trigger REs. Therefore, solely based on the peak slip velocity, it is difficult to determine whether an SSE could trigger a huge earthquake or not. The rupture extent of SSEs is correlated with the occurrence of earthquakes to some extent. The findings in this study may further our understanding of the earthquake cycles and earthquake initiation process.

Conflict of Interest

The authors declare no conflicts of interest relevant to this study.

Data Availability Statement

For reproducibility, numerical models and simulation results of four typical slip behaviors can be found at https://doi.org/10.6084/m9.figshare.19601773.v2.

References

Ariyoshi, K., Matsuzawa, T., Ampuero, J.-P., Nakata, R., Hori, T., Kaneda, Y., et al. (2012). Migration process of very low-frequency events based on a chain-reaction model and its application to the detection of preseismic slip for megathrust earthquakes. *Earth Planets and Space*, *64*(8), 693–702. https://doi.org/10.5047/eps.2010.09.003

Audet, P., Bostock, M. G., Christensen, N. I., & Peacock, S. M. (2009). Seismic evidence for overpressured subducted oceanic crust and megathrust fault sealing. *Nature*, *457*(7225), 76–78. https://doi.org/10.1038/nature07650

Avouac, J.-P. (2015). From geodetic imaging of seismic and aseismic fault slip to dynamic modeling of the seismic cycle. *Annual Review of Earth and Planetary Sciences*, *43*(1), 233–271. https://doi.org/10.1146/annurev-earth-060614-105302

Barbot, S. (2019). Slow slip, slow earthquakes, period-two cycles, full and partial ruptures, and deterministic chaos in a single asperity fault. *Tectonophysics*, *768*, 228171. https://doi.org/10.1016/j.tecto.2019.228171

Bletery, Q., & Nocquet, J. M. (2020). Slip bursts during coalescence of slow slip events in Cascadia. *Nature Communications*, *11*(1), 2159. https://doi.org/10.1038/s41467-020-15494-4

Bürgmann, R. (2018). The geophysics, geology, and mechanics of slow fault slip. *Earth and Planetary Science Letters*, *495*, 112–134. https://doi.org/10.1016/j.epsl.2018.04.062

Dieterich, J. H. (1979). Modeling of rock friction: 1. Experimental results and constitutive equations. *Journal of Geophysical Research*, *84*(B5), 2161–2168. https://doi.org/10.1029/JB084iB05p02161

Dieterich, J. H. (1992). Earthquake nucleation on faults with rate-and state-dependent strength. *Tectonophysics*, *211*(1–4), 115–134. https://doi.org/10.1016/0040-1951(92)90055-b

Dixon, T. H., Jiang, Y., Malservisi, R., McCaffrey, R., Voss, N., Protti, M., & Gonzalez, V. (2014). Earthquake and tsunami forecasts: Relation of slow slip events to subsequent earthquake rupture. *Proceedings of the National Academy of Sciences of the United States of America*, *111*(48), 17039–17044. https://doi.org/10.1073/pnas.1412299111

Dong, P., & Xia, K. (2022). Laboratory investigations probing earthquake source process. *Chinese Science Bulletin*, *67*(13), 1378–1389. https://doi.org/10.1360/tb-2021-1061

Dragert, H., Wang, K., & James, T. S. (2001). A silent slip event on the deeper Cascadia subduction interface. *Science*, *292*(5521), 1525–1528. https://doi.org/10.1126/science.1060152

Dublanchet, P. (2018). The dynamics of earthquake precursors controlled by effective friction. *Geophysical Journal International*, *212*(2), 853–871. https://doi.org/10.1093/gji/ggx438

Fang, Z., Dieterich, J. H., & Xu, G. (2010). Effect of initial conditions and loading path on earthquake nucleation. *Journal of Geophysical Research*, *115*(B6), B06313. https://doi.org/10.1029/2009jb006558

Graham, S. E., DeMets, C., Cabral-Cano, E., Kostoglodov, V., Walpersdorf, A., Cotte, N., et al. (2014). GPS constraints on the 2011–2012 Oaxaca slow slip event that preceded the 20 March 2012 Ometepec earthquake, southern Mexico. *Geophysical Journal International*, *197*(3), 1593–1607. https://doi.org/10.1093/gji/ggu019

Hirose, F., & Maeda, K. (2013). Simulation of recurring earthquakes along the Nankai trough and their relationship to the Tokai long-term slow slip events taking into account the effect of locally elevated pore pressure and subducting ridges. *Journal of Geophysical Research: Solid Earth*, *118*(8), 4127–4144. https://doi.org/10.1002/jgrb.50287

Hirose, H., Hirahara, K., Kimata, F., Fujii, N., & Miyazaki, S. (1999). A slow thrust slip event following the two 1996 Hyuganada earthquakes beneath the Bungo Channel, southwest Japan. *Geophysical Research Letters*, *26*(21), 3237–3240. https://doi.org/10.1029/1999gl010999

Ide, S., Beroza, G. C., Shelly, D. R., & Uchide, T. (2007). A scaling law for slow earthquakes. *Nature*, *447*(7140), 76–79. https://doi.org/10.1038/nature05780

Ito, Y., Obara, K., Shiomi, K., Sekine, S., & Hirose, H. (2007). Slow earthquakes coincident with episodic tremors and slow slip events. *Science*, *315*(5811), 503–506. https://doi.org/10.1126/science.1134454

Kaneko, Y., & Ampuero, J. P. (2011). A mechanism for preseismic steady rupture fronts observed in laboratory experiments. *Geophysical Research Letters*, *38*(21), L21307. https://doi.org/10.1029/2011gl049953

Kaneko, Y., Avouac, J.-P., & Lapusta, N. (2010). Towards inferring earthquake patterns from geodetic observations of interseismic coupling. *Nature Geoscience*, *3*(5), 363–369. https://doi.org/10.1038/ngeo843

Kato, A., & Nakagawa, S. (2014). Multiple slow slip events during a foreshock sequence of the 2014 Iquique, Chile Mw 8.1 earthquake. *Geophysical Research Letters*, *41*(45), 5420–5427. https://doi.org/10.1002/2014GL061138

Kato, A., Obara, K., Igarashi, T., Tsuruoka, H., Nakatani, M., & Hirata, N. (2012). Propagation of slow slip leading up to the 2011 Mw 9.0 Tohoku-Oki earthquake. *Science*, *335*(6069), 705–708. https://doi.org/10.1126/science.1215141

Kato, N. (2003). A possible model for large preseismic slip on a deeper extension of a seismic rupture plane. *Earth and Planetary Science Letters*, *216*(1–2), 17–25. https://doi.org/10.1016/S0012-821X(03)00483-7

Kato, N. (2004). Interaction of slip on asperities: Numerical simulation of seismic cycles on a two-dimensional planar fault with nonuniform frictional property. *Journal of Geophysical Research*, *109*(B12), B12306. https://doi.org/10.1029/2004jb003001

Kato, N. (2020). Complexity in the earthquake cycle increases with the number of interacting patches. *Pure and Applied Geophysics*, *177*(10), 4657–4676. https://doi.org/10.1007/s00024-020-02555-4

Khoshmanesh, M., & Shirzaei, M. (2018). Episodic creep events on the San Andreas Fault caused by pore-pressure variations. *Nature Geoscience*, *11*(8), 610–614. https://doi.org/10.1038/s41561-018-0160-2

Khoshmanesh, M., Shirzaei, M., & Nadeau, R. M. (2015). Time-dependent model of aseismic slip on the central San Andreas Fault from InSAR time series and repeating earthquakes. *Journal of Geophysical Research: Solid Earth*, *120*(9), 6658–6679. https://doi.org/10.1002/2015jb012039

Kodaira, S., Iidaka, T., Kato, A., Park, J.-O., Iwasaki, T., & Kaneda, Y. (2004). High pore fluid pressure may cause silent slip in the Nankai trough. *Science*, *304*(5675), 1295–1298. https://doi.org/10.1126/science.1096535

Latour, S., Schubnel, A., Nielsen, S., Madariaga, R., & Vinciguerra, S. (2013). Characterization of nucleation during laboratory earthquakes. *Geophysical Research Letters*, *40*(19), 5064–5069. https://doi.org/10.1002/grl.50974

Lavier, L. L., Tong, X., & Biemiller, J. (2021). The mechanics of creep, slow slip events, and earthquakes in mixed brittle-ductile fault zones. *Journal of Geophysical Research: Solid Earth*, *126*(2), e2020JB020325. https://doi.org/10.1029/2020jb020325

Li, D., & Liu, Y. (2017). Modeling slow slip segmentation in Cascadia subduction zone constrained by tremor locations and gravity anomalies. *Journal of Geophysical Research: Solid Earth*, *122*(4), 3138–3157. https://doi.org/10.1002/2016jb013778

Linde, A. T., Gladwin, M. T., Johnston, M. J., Gwyther, R. L., & Bilham, R. G. (1996). A slow earthquake sequence on the San Andreas Fault. *Nature*, *383*(6595), 65–68. https://doi.org/10.1038/383065a0

Liu, Y., & Rice, J. R. (2005). Aseismic slip transients emerge spontaneously in three-dimensional rate and state modeling of subduction earthquake sequences. *Journal of Geophysical Research*, *110*(B8), B08307. https://doi.org/10.1029/2004jb003424

Liu, Y., & Rice, J. R. (2007). Spontaneous and triggered aseismic deformation transients in a subduction fault model. *Journal of Geophysical Research*, *112*(B9), B09404. https://doi.org/10.1029/2007jb004930

Liu, Y., & Rubin, A. M. (2010). Role of fault gouge dilatancy on aseismic deformation transients. *Journal of Geophysical Research*, *115*(B10), B10310. https://doi.org/10.1029/2010jb007522

Luo, Y., & Ampuero, J.-P. (2018). Stability of faults with heterogeneous friction properties and effective normal stress. *Tectonophysics*, *733*, 257–272. https://doi.org/10.1016/j.tecto.2017.11.006

Luo, Y., & Liu, Z. (2019). Slow-slip recurrent pattern changes: Perturbation responding and possible scenarios of precursor toward a megathrust earthquake. *Geochemistry, Geophysics, Geosystems*, *20*(2), 852–871. https://doi.org/10.1029/2018gc008021

Luo, Y., & Liu, Z. (2021). Fault zone heterogeneities explain depth-dependent pattern and evolution of slow earthquakes in Cascadia. *Nature Communications*, *12*(1), 1959. https://doi.org/10.1038/s41467-021-22232-x

Matsuzawa, T., Hirose, H., Shibazaki, B., & Obara, K. (2010). Modeling short- and long-term slow slip events in the seismic cycles of large subduction earthquakes. *Journal of Geophysical Research*, *115*(B12), B12301. https://doi.org/10.1029/2010jb007566

Mazzotti, S., & Adams, J. (2004). Variability of near-term probability for the next great earthquake on the Cascadia subduction zone. *Bulletin of the Seismological Society of America*, *94*(5), 1954–1959. https://doi.org/10.1785/012004032

Michel, S., Gualandi, A., & Avouac, J.-P. (2018). Interseismic coupling and slow slip events on the Cascadia megathrust. *Pure and Applied Geophysics*, *176*(9), 3867–3891. https://doi.org/10.1007/s00024-018-1991-x

Miller, M. M., Melbourne, T., Johnson, D. J., & Sumner, W. Q. (2002). Periodic slow earthquakes from the Cascadia subduction zone. *Science*, *295*(5564), 2423. https://doi.org/10.1126/science.1071193

Nadeau, R. M., & McEvilly, T. V. (2004). Periodic pulsing of characteristic microearthquakes on the San Andreas Fault. *Science*, *303*(5655), 220–222. https://doi.org/10.1126/science.1090353

Nielsen, S., Taddeucci, J., & Vinciguerra, S. (2010). Experimental observation of stick-slip instability fronts. *Geophysical Journal International*, *180*(2), 697–702. https://doi.org/10.1111/j.1365-246X.2009.04444.x

Noda, H., Nakatani, M., & Hori, T. (2013). Large nucleation before large earthquakes is sometimes skipped due to cascade-up-Implications from a rate and state simulation of faults with hierarchical asperities. *Journal of Geophysical Research: Solid Earth*, *118*(6), 2924–2952. https://doi.org/10.1002/jgrb.50211

Obara, K., & Kato, A. (2016). Connecting slow earthquakes to huge earthquakes. *Science*, *353*(6296), 253–257. https://doi.org/10.1126/science.aaf1512

Ohnaka, M., & Kuwahara, Y. (1990). Characteristic features of local breakdown near a crack-tip in the transition zone from nucleation to unstable rupture during stick-slip shear failure. *Tectonophysics*, *175*(1), 197–220. https://doi.org/10.1016/0040-1951(90)90138-x

Ohtani, M., Hirahara, K., Hori, T., & Hyodo, M. (2014). Observed change in plate coupling close to the rupture initiation area before the occurrence of the 2011 Tohoku earthquake: Implications from an earthquake cycle model. *Geophysical Research Letters*, *41*(6), 1899–1906. https://doi.org/10.1002/2013gl058751

Ohtani, M., Kame, N., & Nakatani, M. (2019). Nucleation of characteristic earthquakes in simulated cycles involving deep huge slow slip events. *Journal of Geophysical Research: Solid Earth*, *124*(2), 1822–1837. https://doi.org/10.1029/2018jb016156

Ozawa, S. (2014). Shortening of recurrence interval of Boso slow slip events in Japan. *Geophysical Research Letters*, *41*(8), 2762–2768. https://doi.org/10.1002/2014gl060072

Ozawa, S., Murakami, M., Kaidzu, M., Tada, T., Sagiya, T., Hatanaka, Y., et al. (2002). Detection and monitoring of ongoing aseismic slip in the Tokai region, Central Japan. *Science*, *298*(5595), 1009–1012. https://doi.org/10.1126/science.1076780

Peng, Z., & Gomberg, J. (2010). An integrated perspective of the continuum between earthquakes and slow slip phenomena. *Nature Geoscience*, *3*(9), 599–607. https://doi.org/10.1038/ngeo940

Perfettini, H., Avouac, J. P., Tavera, H., Kositsky, A., Nocquet, J. M., Bondoux, F., et al. (2010). Seismic and aseismic slip on the Central Peru megathrust. *Nature*, *465*(7294), 78–81. https://doi.org/10.1038/nature09062

Presse, W. H., Teukolsky, S. A., Vetterling, W. T., & Flannery, B. P. (1992). *Numerical recipes in C: The art of scientific computing* (2nd ed.). Cambridge University Press.

Radiguet, M., Cotton, F., Vergnolle, M., Campillo, M., Walpersdorf, A., Cotte, N., & Kostoglodov, V. (2012). Slow slip events and strain accumulation in the Guerrero gap, Mexico. *Journal of Geophysical Research: Solid Earth*, *117*(B4), B04305. https://doi.org/10.1029/2011jb008801

Radiguet, M., Perfettini, H., Cotte, N., Gualandi, A., Valette, B., Kostoglodov, V., et al. (2016). Triggering of the 2014 Mw 7.3 Papanoa earthquake by a slow slip event in Guerrero, Mexico. *Nature Geoscience*, *9*(11), 829–833. https://doi.org/10.1038/ngeo2817

Rice, J. R. (1993). Spatio-temporal complexity of slip on a fault. *Journal of Geophysical Research*, *98*(B6), 9885–9907. https://doi.org/10.1029/93jb00191

Rogers, G., & Dragert, H. (2003). Episodic tremor and slip on the Cascadia subduction zone: The chatter of silent slip. *Science*, *300*(5627), 1942–1943. https://doi.org/10.1126/science.1084783

Rolandone, F., Nocquet, E.-M., Mothes, P. A., Jarrin, P., Vallée, M., Cubas, N., et al. (2018). Areas prone to slow slip events impede earthquake rupture propagation and promote afterslip. *Science Advances*, *4*(1), eaao6596. https://doi.org/10.1126/sciadv.aao6596

Rubin, A. M., & Ampuero, J. P. (2005). Earthquake nucleation on (aging) rate and state faults. *Journal of Geophysical Research*, *110*(B11), B11312. https://doi.org/10.1029/2005jb003686

Rubin, A. M., & Ampuero, J.-P. (2009). Self-similar slip pulses during rate-and-state earthquake nucleation. *Journal of Geophysical Research*, *114*(B11), B11305. https://doi.org/10.1029/2009jb006529

Ruina, A. (1983). Slip instability and state variable friction laws. *Journal of Geophysical Research*, *88*(B12), 10359–10370. https://doi.org/10.1029/JB088iB12p10359

Ruiz, S., Metois, M., Fuenzalida, A., Ruiz, J., Leyton, F., Grandin, R., et al. (2014). Intense foreshocks and a slow slip event preceded the 2014 Iquique Mw 8.1 earthquake. *Science*, *345*(6201), 1165–1169. https://doi.org/10.1126/science.1256074

Saffer, D. M. (2017). Mapping fluids to subduction megathrust locking and slip behavior. *Geophysical Research Letters*, *44*(18), 9337–9340. https://doi.org/10.1002/2017gl075381

Saltogianni, V., Mouslopoulou, V., Dielforder, A., Bocchini, G. M., Bedford, J., & Oncken, O. (2021). Slow slip triggers the 2018 Mw 6.9 Zakynthos earthquake within the weakly locked Hellenic Subduction System, Greece. *Geochemistry, Geophysics, Geosystems*, *22*(11). https://doi.org/10.1029/2021gc010090

Scholz, C. H. (1998). Earthquakes and friction laws. *Nature*, *391*(6662), 37–42. https://doi.org/10.1038/34097

Segall, P., & Bradley, A. M. (2012). Slow slip evolves into megathrust earthquakes in 2D numerical simulations. *Geophysical Research Letters*, *39*(18), L18308. https://doi.org/10.1029/2012gl052811

Shelly, D. R. (2009). Possible deep fault slip preceding the 2004 Parkfield earthquake, inferred from detailed observations of tectonic tremor. *Geophysical Research Letters*, *36*(17), L17318. https://doi.org/10.1029/2009gl039589

Shelly, D. R., Beroza, G. C., Ide, S., & Nakamula, S. (2006). Low-frequency earthquakes in Shikoku, Japan, and their relationship to episodic tremor and slip. *Nature*, *442*(7099), 188–191. https://doi.org/10.1038/nature04931

Shibazaki, B., Bu, S., Matsuzawa, T., & Hirose, H. (2010). Modeling the activity of short-term slow slip events along deep subduction interfaces beneath Shikoku, southwest Japan. *Journal of Geophysical Research*, *115*, B00A19. https://doi.org/10.1029/2008jb006057

Shibazaki, B., & Shimamoto, T. (2007). Modeling of short-interval silent slip events in deeper subduction interfaces considering the frictional properties at the unstable-stable transition regime. *Geophysical Journal International*, *171*(1), 191–205. https://doi.org/10.1111/j.1365-246X.2007.03434.x

Shibazaki, B., Wallace, W. K., Kaneko, Y., Hamling, I. J., Ito, H., & Matsuzawa, T. (2019). Three-dimensional modeling of spontaneous and triggered slow-slip events at the Hikurangi Subduction Zone, New Zealand. *Journal of Geophysical Research: Solid Earth*, *124*(13), 13250–13268. https://doi.org/10.1029/2019JB018190

Skarbek, R. M., Rempel, A. W., & Schmidt, D. A. (2012). Geologic heterogeneity can produce aseismic slip transients. *Geophysical Research Letters*, *39*(21), L21306. https://doi.org/10.1029/2012gl053762

Socquet, A., Valdes, J. P., Jara, J., Cotton, F., Walpersdorf, A., Cotte, N., et al. (2017). An 8 months slow slip event triggers progressive nucleation of the 2014 Chile megathrust. *Geophysical Research Letters*, *44*(9), 4046–4053. https://doi.org/10.1002/2017gl073023

Uchida, N., Iinuma, T., Nadeau, R. M., Bürgmann, R., & Hino, R. (2016). Periodic slow slip triggers megathrust zone earthquakes in northeastern Japan. *Science*, *351*(6272), 488–492. https://doi.org/10.1126/science.aad3108

Uchida, N., Takagi, R., Asano, Y., & Obara, K. (2020). Migration of shallow and deep slow earthquakes toward the locked segment of the Nankai megathrust. *Earth and Planetary Science Letters*, *531*, 115986. https://doi.org/10.1016/j.epsl.2019.115986

Veedu, D. M., & Barbot, S. (2016). The Parkfield tremors reveal slow and fast ruptures on the same asperity. *Nature*, *532*(7599), 361–365. https://doi.org/10.1038/nature17190

Voss, N., Dixon, T. H., Liu, Z., Malservisi, R., Protti, M., & Schwartz, S. (2018). Do slow slip events trigger large and great megathrust earthquakes? *Science Advances*, *4*(10), eaat8472. https://doi.org/10.1126/sciadv.aat8472

Wallace, L. M., Webb, S. C., Ito, Y., Mochizuki, K., Hino, R., Henrys, S., et al. (2016). Slow slip near the trench at the Hikurangi subduction zone, New Zealand. *Science*, *352*(6286), 701–704. https://doi.org/10.1126/science.aaf2349

Wei, M., Kaneko, Y., Liu, Y., & McGuire, J. J. (2013). Episodic fault creep events in California controlled by shallow frictional heterogeneity. *Nature Geoscience*, *6*(7), 566–570. https://doi.org/10.1038/ngeo1835

Weng, H., Huang, J., & Yang, H. (2015). Barrier-induced supershear ruptures on a slip-weakening fault. *Geophysical Research Letters*, *42*(12), 4824–4832. https://doi.org/10.1002/2015GL064281

Wu, Y., & Chen, X. (2014). The scale-dependent slip pattern for a uniform fault model obeying the rate- and state-dependent friction law. *Journal of Geophysical Research: Solid Earth*, *119*(6), 4890–4906. https://doi.org/10.1002/2013jb010779

Yabe, S., & Ide, S. (2018). Variations in precursory slip behavior resulting from frictional heterogeneity. *Progress in Earth and Planetary Science*, *5*(1), 43. https://doi.org/10.1186/s40645-018-0201-x

Yang, H., Liu, Y., & Lin, J. (2012). Effects of subducted seamounts on megathrust earthquake nucleation and rupture propagation. *Geophysical Research Letters*, *39*(24), L24302. https://doi.org/10.1029/2012gl053892

Yang, H., Liu, Y., & Lin, J. (2013). Geometrical effects of a subducted seamount on stopping megathrust ruptures. *Geophysical Research Letters*, *40*(10), 2011–2016. https://doi.org/10.1002/grl.50509

Yang, H., Yao, S., & Chen, X. (2022). Rupture propagation on heterogeneous fault: Challenges for predicting earthquake magnitude. *Chinese Science Bulletin*, *67*(13), 1–14. https://doi.org/10.1360/tb-2021-1086

Yang, H., Yao, S., He, B., & Newman, A. V. (2019). Earthquake rupture dependence on hypocentral location along the Nicoya Peninsula subduction megathrust. *Earth and Planetary Science Letters*, *520*, 10–17. https://doi.org/10.1016/j.epsl.2019.05.030

Yang, H., Yao, S., He, B., Newman, A. V., & Weng, H. (2019). Deriving rupture scenarios from interseismic locking distributions along the subduction megathrust. *Journal of Geophysical Research: Solid Earth*, *124*(10), 10376–10392. https://doi.org/10.1029/2019jb017541

Yao, S., & Yang, H. (2020). Rupture dynamics of the 2012 Nicoya Mw 7.6 earthquake: Evidence for low strength on the megathrust. *Geophysical Research Letters*, *47*(13), e2020GL087508. https://doi.org/10.1029/2020gl087508

Yao, S., & Yang, H. (2022). Hypocentral dependent shallow slip distribution and rupture extents along a strike-slip fault. *Earth and Planetary Science Letters*, *578*, 117296. https://doi.org/10.1016/j.epsl.2021.117296

Yokota, Y., & Koketsu, K. (2015). A very long-term transient event preceding the 2011 Tohoku earthquake. *Nature Communications*, *6*(1), 6934. https://doi.org/10.1038/ncomms6934

Zhu, W., Allison, K. L., Dunham, E. M., & Yang, Y. (2020). Fault valving and pore pressure evolution in simulations of earthquake sequences and aseismic slip. *Nature Communications*, *11*(1), 4833. https://doi.org/10.1038/s41467-020-18598-z